國立政治大學理學院應用物理研究所

碩士論文

Graduate Institute of Applied Physics, College of Science

National Chengchi University

Master Thesis

利用第一原理計算研究多鐵氧化物 $Cu_3Mo_2O_9$ 的磁性, 電子態及鐵電性質

Ab Initio Studies of The Magnetic, Electronic and Ferroelectric Properties of Multiferroic Oxide $Cu_3Mo_2O_9$

蕭逸修

Yi-Hsiu Hsiao

指導教授：郭光宇 博士

Advisor : Guang-Yu Guo, Ph.D.

中華民國一〇一年九月

September, 2012

Abstract

In this thesis, we used the *ab initio* method to study a multiferroic oxide $Cu_3Mo_2O_9$. The correlations of electrons must be considered in this system so that a reasonable energy gap can be obtained. Due to the geometric frustration of magnetic structure caused by crystal structure, the ground state spin configuration in this system still has not been determined experimentally. We found some spin configurations similar to the non-collinear anti-ferromagnetic spins configuration suggested by Vilminot et al.. Competition between exchange interactions and spin-orbit coupling effect determines the canting of spins on Cu atoms. The calculated exchange parameters agree with the experimental results well. By using Berry phase calculations, we obtained the theoretical value of spontaneous electric polarization. The strength of polarization in our results is in the same order of results of experiments. However, the direction of electric polarization we found (along b-axis) is different from the experimental measurements (along c-axis). We have found a spin configuration that the theoretical electric polarization of the state agrees with the experimental results. However, the symmetry of the spin configuration does not satisfy the conditions suggested by results of the neutron diffraction experiment. And, spins on neighboring Cu2 and Cu3 do not form a singlet dimer. Since there still is no *ab initio* calculation studying this oxide, we hope that our studies can help those who are also interested in this material.

中文摘要

在此論文中，我們利用第一原理計算研究多鐵材料 $Cu_3Mo_2O_9$ 的磁性、電子態及多鐵性質。我們發現在此系統中，電子與電子間的庫倫排斥力必須被考慮，以致於導帶與價帶間能隙能夠被良好地描述。由於晶體結構所導致的幾何不穩定性，系統的磁結構尚未在實驗測量中被確定。在我們的理論計算當中得到的磁結構與 Vilminot 等研究人員根據實驗結果猜測出的非線性反鐵磁結構類似。交換作用與自旋軌道耦合間的爭競決定了電子自旋方向的傾斜。計算所得到的交換作用係數與實驗結果吻合良好。利用 Berry's phase 計算，我們得到了系統自發電極化的理論值，其強度與實驗量測值在同一個數量級。然而，在我們計算中得到的電極化方向(平行於 b 軸)與實驗(平行於 c 軸)不符。此外，我們發現一磁結構之理論電極化方向與實驗相符，然而其磁結構之對稱性與實驗不符。目前，尚未有第一原理計算研究此氧化物，我們希望此論文能夠對同樣有興趣研究此材料的研究人員有所幫助。

Contents

List of Figures

List of Tables

Chapter 1

Introduction

As a relatively new course, the computational physics can be traced back to 1960s. At that time, extensive applications of quantum mechanics and discovery of complicated molecular like double helix structure of DNA motivated scientists using computers as a tool to study interactions and mechanism in the macromolecules. With the developement of technology of computer, objects of study transit from atomic and molecular levels to the large-scale condensed matter systems. The computational physics becomes a new branch of physical studies in addition to theoretical and experimental physics up to now. Here we only introduce the *ab initio* method in this thesis. The so-called "*ab initio*" means that there needs no any empirical parameters. The calculation starts directly at the level of established laws of physics, i.e. the quantum mechanics. What we have to do is to input the position of atoms in an unit cell. Though there are phenomena which cannot be described, the *ab initio* method still gains lots of achievements irrefutably that some behaviors in the material can be explained or predicted.

An interesting multiferroics, $Cu_3Mo_2O_9$, with strong magnetoelectric coupling has attractted our attention. The origin of the electricity of this material may probably be a novel mechanism. A small spin cluster model has been suggested by Kuroe et al. which is very different from the magnetic superlattice. Since there still has no *ab initio* calculation to study it, we performed a series of calculations based on spin density functional theory. The traditional DFT and the DFT+U method consisting of in a Hubbard-like correction which gives a better description of electronic correlation will be introduced in chapter 2. The crystal field theory introduced in chapter 3 helps us a lot analysing the electronic structure of $Cu_3Mo_2O_9$. It can describe the way of the splitting of d-orbitals to explain colors, strength of magnetic moment and structural distortion of transition metal complexes. The overview of multiferroics in chapter 4 describes many mechanisms of ferroelectricity, type-I (weak or no magnetoelectric coupling) and type-II (strong magnetoelectric coupling) multiferroics. In chapter 5, we discuss results in our calculations including the magnetic structure, electronic structure and spontaneous electric polarization of the system. Finally, summary and conclusions will be given in chapter 6.

Chapter 2

Density Functional Theory

The density functional theory (DFT) is one of the most successful approach describing the properties of matters in the ground state. It was introduced in two seminal papers by Hohenberg-Kohn (1964) [1] and Kohn-Sham (1965) [2]. Walter Kohn was awarded with the Nobel Prize in Chemistry in 1998. The main idea of DFT is that it describes a many-electron system as a single electron moving in the pseudopotential, i.e. wavefunction of electrons represented as a functional of the electron density depends on spatial position. Only three degrees of freedom makes it possible to simulate the more complex system (larger number of particles) than before. It acquires the considerable achievement in material calculation science that some difficult question could be answered and some precursory material could be predicted.

2.1 Born-Oppenheimer approximation

Thanks to the developement of quantum mechanics, we can describe those behaviors in the microscopic scale that Newton's mechanics cannot explain. To solve a problem of condensed matter physics, we write down the Hamiltonian correspond to the system,

$$\begin{aligned} H = &-\sum_{I=1}^{N}\frac{\hbar^2}{2M_I}\nabla_I^2+\frac{1}{2}\sum_{I\neq J}^{N}\frac{Z_I Z_J e^2}{4\pi\varepsilon_0\left|R_I-R_J\right|} \\ &-\frac{\hbar^2}{2m}\sum_{i=1}^{n}\nabla_i^2+\frac{1}{2}\sum_{i\neq j}^{n}\frac{e^2}{4\pi\varepsilon_0\left|r_i-r_j\right|}-\frac{1}{4\pi\varepsilon_0}\sum_{i=1}^{n}\sum_{I=1}^{N}\frac{Z_I e^2}{\left|r_i-R_I\right|}, \end{aligned} \tag{2.1}$$

where N and n are numbers of nuclei and electrons respectively. M and m are masses of nucleus and electron respectively. Ze and e are charges of nuclei and electrons respectively. R and r are positions of nucleus and electron respectively, and $\hbar$ is the reduced Planck constant and ε_0 is the vacuum permittivity. The Hamiltonian above includes the kinetic energy of nuclei and electrons, and the Coulomb potential energy of nucleus-nucleus, electron-electron and nucleus-electron interactions. Now we can solve the Schrodinger equation to obtain the wavefunction of

the system,

$$H\psi(r_1, r_2, ..., r_n, R_1, R_2, ..., R_N) = E\psi(r_1, r_2, ..., r_n, R_1, R_2, ..., R_N) \tag{2.2}$$

where ψ is the eigenfunction of the operator H corresponds to energy E. However, it is diffcult to deal with such complex equation including N nuclei and n electrons components. A preliminary method to simplify the problem is the Born-Oppenheimer approximation proposed in 1927 [3], also called the adiabatic approach, describing the seperation of electronic motion, nuclear vibrations, and molecular rotation. Since any nucleus is much more massive than an electron, it must accordingly have much smaller velocities, about two orders of time scale larger than electrons. The electrons that move around the nuclei in the system have enough time to reach the ground state as the nuclei undergo a small perturbation. Therefore, the system now can be seen that electrons moving in the arrangement of stationary nuclei. The Hamiltonian H then becomes

$$H = H_n + H_e \tag{2.3}$$

where H_n is the nucleus part including the first two terms of equation 2.1, and H_e is the electron part including the remaining three terms. The wavefunction seperated into two parts,

$$\psi(r_1, r_2, ..., r_n, R_1, R_2, ..., R_N) = \psi_n(R_1, R_2, ..., R_N) \times \psi_e(r_1, r_2, ..., r_n), \tag{2.4}$$

and

$$\begin{aligned} &(H_n + H_e)\psi_n(R_1, R_2, ..., R_N) \times \psi_e(r_1, r_2, ..., r_n) \\ &= (E_n + E_e)\psi_n(R_1, R_2, ..., R_N) \times \psi_e(r_1, r_2, ..., r_n), \end{aligned} \tag{2.5}$$

then the wavefunction of electrons can be discussed separately. However, although the problem has been simplified, it is still too complicated to solve. Some theories proposed for simplifying the problem further. In the Thomas-Fermi theory, the precursory idea that the wavefunction of electrons is represented as a functional of the electronic density, which is proposed by Llewellyn Thomas and Enrico Fermi in 1927 [4] and will be discussed in the next section. And in the Hartree-Fock theory proposed in 1930, every electron moves in the mean field caused by other electrons. The Hamiltonian of the many-body system is decomposed into a sum of Hamiltonians of several one-body systems, and this theory will not be discussed in the following.

2.2 Thomas-Fermi Theory

The Thomas-Fermi theory [4], which was the forerunner of the DFT, suggests a precursory idea that wavefunction of electrons is represented as a functional of the electronic density,

$$\rho(r) = \rho(r_1) = n \int \psi^*(r_1, r_2, ..., r_n)\psi(r_1, r_2, ..., r_n) dr_2 ... dr_n, \tag{2.6}$$

where ρ, n and ψ are the density, number and wavefunction of electrons respectively. To realize the theory, we firstly consider a box of stationary and uniform electrons. States must be occupied in turn from the ground state to the highest occupied state correspond to the wavenumber k_F which is related to the density,

$$3\pi^2\rho = k_F^3, \tag{2.7}$$

and the kinetic energy of the electrons is

$$T = \frac{\Omega}{\pi^2}\frac{\hbar^2}{10m}k_F^2, \tag{2.8}$$

where Ω is the volume of the box. Now we go back to the real system. A non-uniform system is seen locally uniform. The density and wavenumber are functions of the position. Thus the kinetic energy of electrons within the Thomas-Fermi theory is

$$T[\rho] = \int d^3r \frac{3}{5}\frac{\hbar^2 k_F^2(r)}{2m}\rho(r). \tag{2.9}$$

Here we must notice that this kinetic term is associated with the non-interacting electrons. The Coulomb potential energy of the nucleus-electron and the electron-electron interactions are

$$U_{nu-e}[\rho] = \int \rho(r)V_{nu}(r)d^3r \quad and \quad U_{e-e}[\rho] = \frac{1}{2}e^2\int \frac{\rho(r)\rho(r')}{|r-r'|}d^3rd^3r', \tag{2.10}$$

and the total energy is

$$E[\rho] = T[\rho] + U_{nu-e}[\rho] + U_{e-e}[\rho]. \tag{2.11}$$

A many-body Schrodinger equation can successfully be simplifed into a one-body Schrodinger equation. It is a large step of achievement that the equation is simple enough to be solved. However, the accuracy of the method above is limited. Because the kinetic energy term is oversimplified that it consider the electrons as the non-interacting Fermi gas, the exchange-correlation of electrons are completely neglected. There are interactions between electrons respect to spin called the exchange interaction. It lowers the total energy further, since it makes electrons more apart. The physist Dirac tried to add an exchange term into the equation, but still failled because of that the kinetic term which see electrons as a uniform gas is conceptually a big error, and the correlation of electrons is completely neglected.

2.3 Density Functional Theory

Although the concept of the functional of the electronic density can be traced back to the Thomas-Fermi theory in 1927 [4], the confirmed theoretical foundation, the Hohenberg-Kohn Theorem, is not proposed till 1964 by Hohenberg and Kohn [1]. However, it does not provide a way of finding the electronic density in the ground state. By employing the Kohn-Sham equation

proposed in 1965 [2], the ground state density is able to be found and the density functional theory gains the incomparable achievement in physics and chemistry from this moment on. The complete discussion will be in the following subsections.

2.3.1 Hohenberg-Kohn Theorem

There are two theorems proposed and proved by Hohenberg and Kohn as follows.

The First Hohenberg-Kohn theorem

The first theorem demonstrates that the Hamiltonian and all the properties of the system are uniquely determined by the electron density. The proof is derived in the following. Assume that there are two different external potentials generated by a set of nuclei, $V_1(r)$ and $V_2(r)$, we would have two different Hamiltonians, H_1 and H_2, each leads to the same $\rho(r)$ for its ground state, but the two corresponding wavefunctions, $\psi_1(r)$ and $\psi_2(r)$, are different. Now we take ψ_2 as a trial wave function for the problem of the Hamiltonian H_1,

$$E_1 < \langle \psi_2 | H_1 | \psi_2 \rangle = \langle \psi_2 | H_2 | \psi_2 \rangle + \langle \psi_2 | H_1 - H_2 | \psi_2 \rangle = E_2 + \int \rho(r)[V_1(r) - V_2(r)]dr, \quad (2.12)$$

where E_1 and E_2 are eigenenergies of H_1 and H_2 respectively. Similarly, we take ψ_1 as a trial wave function for the problem of the Hamiltonian H_2,

$$E_2 < \langle \psi_1 | H_2 | \psi_1 \rangle = \langle \psi_1 | H_1 | \psi_1 \rangle + \langle \psi_1 | H_2 - H_1 | \psi_1 \rangle = E_1 + \int \rho(r)[V_2(r) - V_1(r)]dr. \quad (2.13)$$

Adding Eq. (2.12) and (2.13), we would obtain a contradictory relation,

$$E_1 + E_2 < E_2 + E_1. \quad (2.14)$$

The first Hohenberg-Kohn theorem is proved that no two different external potentials can give the same electron density for the ground state. The total energy is a unique functional of the electron density which can be written as

$$E[\rho] = T[\rho] + U_{n-e}[\rho] + U_{e-e}[\rho], \quad (2.15)$$

where T and U_{n-e} are kinetic energy and nucleus-electron Coulomb potential energy. And the U_{e-e} here that differs from the term of Thomas-Fermi theory is the energy related to the electron-electron interaction including the electron-electron Coulomb repulsion, exchange interaction and Coulomb correlation.

The Second Hohenberg-Kohn Theorem

As follows , the second Hohenberg-Kohn theorem, the variation principle, enable us to make sure that the ground state density is what we are looking for. Recall that any trial electron density ρ_1 defines its own Hamiltonian H_1 and hence its own wavefunction ψ_1. The wavefunction can now be taken as the trial wavefunction for the Hamiltonian H_0 generated by the external potential V_{ext}. Thus,

$$\langle \psi_1 | H_0 | \psi_1 \rangle = T[\rho_1] + U_{nu-e}[\rho_1] + U_{e-e}[\rho_1] = E[\rho_1] \geq E[\rho_0] = \langle \psi_0 | H_0 | \psi_0 \rangle = E_0, \quad (2.16)$$

the functional $E[\rho]$ has its minimum relative to variations $\delta\rho$ of the density at the equilibrium density ρ_0,

$$\frac{\delta E[\rho]}{\delta \rho}|_{\rho=\rho_0} = 0. \quad (2.17)$$

2.3.2 Kohn-Sham Equation

The kinetic energy has a large contribution to the total energy. The failure of the Thomas-Fermi theory is due to that it makes the wrong approximation of the term of kinetic energy. The density functional theory, therefore, was ignored until Kohn and Sham introduced a method which treated the majority of the kinetic energy exactly. The theory begins by considering the non-interacting reference system that all electrons move in an effective potential with no interaction, in other words, a mean field single particle picture. The ground state is a Slater determinant of orthogonal orbitals ψ_i which satisfies the equations

$$[-\frac{\hbar^2}{2m}\nabla^2 + V_{eff}(r)]\psi_i(r) = E_i(r)\psi_i(r) \quad with \quad \sum_{i=1}^{n} |\psi_i(r)|^2 = \rho(r), \quad (2.18)$$

where V_{eff} is the effective potential including the nucleus-electron, electron-electron Coulomb term and the ill-defined exchange-correlation term, and n is the number of electrons. Due to the Hohenberg-Kohn theorem, the kinetic energy and total energy are given by

$$T[\rho] = \sum_{i=1}^{n} \int \psi_i^*(r)(-\frac{\hbar^2}{2m}\nabla^2)\psi_i(r)dr \quad and \quad E[\rho] = T[\rho] + \int \rho(r)V_{eff}(r)dr. \quad (2.19)$$

The functional $T[\rho]$ is just a particular case, the ground state electron density now can equivalently be obtained by the solution of th Euler-Lagrange equations,

$$0 = \frac{\delta}{\delta\rho(r)}\left[E[\rho] - \mu_s \int \rho(r)dr\right] = \frac{\delta T[\rho]}{\delta\rho} + V_{eff}(r) - \mu_s, \quad (2.20)$$

where the Lagrange multiplier μ_s satisfies the constraint that the density integrates to the correct number of electrons. It is very important to realize that if the exact form of exchange-correlation term in the effective potential can be defined, the Kohn-Sham strategy would lead to the exact

energy. This will be briefly discussed in the next section.

2.3.3 Exchange-Correlation Energy

Since the work of Kohn and Sham, the remaining question is the available form of the exchange-correlation term of the effective potential,

$$V_{eff}(r) = V_{ext}(r) + \int \frac{\rho(r')}{|r-r'|}dr' + V_{XC}(r) \quad and \quad V_{XC}(r) = \frac{\delta E_{XC}[\rho(r)]}{\delta(r)}, \tag{2.21}$$

where E_{XC} is the exchange-correlation energy. Some successful methods of exchange-correlation approximation like the local density approximation (LDA) [5] and generalized gradient approximation (GGA) [6] are briefly introduced in the following. By the way, the Perdew-Burke-Ernzerhof exchange-correlation functional (PBE) [7] is used in our calculations.

The Local Density Approximation (LDA)

Local density approximation [5], the basis of all approximate exchange-correlation functionals, is the simplest and the most widely used one. The central idea of this approximation is the well-defined limit of exchange-correlation energy of the uniform electron gas. A non-uniform system can be seen as a locally uniform system, and the exchange-correlation energy is

$$E_{XC}^{LDA}[\rho(r)] = \int \rho(r)\varepsilon_{XC}[\rho(r)]dr, \tag{2.22}$$

where $\varepsilon_{XC}[\rho(r)]$ is the exchange-correlation energy per electron of an uniform electron gas of density $\rho(r)$. The quantity $\varepsilon_{XC}[\rho(r)]$ can be further seperated into two parts, exchange and correlation terms,

$$\varepsilon_{XC}[\rho(r)] = \varepsilon_X[\rho(r)] + \varepsilon_C[\rho(r)]. \tag{2.23}$$

The exchange part was originally derived by Bloch and Dirac where

$$\varepsilon_X[\rho(r)] = -\frac{3}{4}(\frac{3\rho(r)}{\pi})^{1/3}. \tag{2.24}$$

However, there has no explicit form for the correlation part, but the numerical quantum Monte-Carlo simulations of the uniform electron gas with good accuracy. It is able to introduce the spin to the LDA (LSDA), and the form becomes

$$E_{XC}^{LSDA}[\rho_\uparrow(r), \rho_\downarrow(r)] = \int \rho(r)\varepsilon_{XC}[\rho_\uparrow(r), \rho_\downarrow(r)]dr. \tag{2.25}$$

The accuracy of the L(S)DA is limited. Only materials with slowly varying electron density can be describe well. However, some bulk and surface of solids exist the rapid varying density. For some materials that have strongly correlated d or f electrons, L(S)DA even predicts them to

be metallic instead of insulating ground state. It tends to underestimate the ground state energy, band gap and the ionization energies, but overestimates the bonding energy.

The Generalized Gradient Approximation (GGA)

To promote the accuracy, not only $\rho(r)$ but also the gradient of $\rho(r)$ are considered to account the exchange-correlation energy since the fact that the electron density of a real system is non-uniform. The form of exchange-correlation energy in the generalized gradient approximation [6] can be expressed as

$$E_{XC}^{GGA}[\rho_{\uparrow}(r),\rho_{\downarrow}(r)] = \int \rho(r)\varepsilon_{XC}[\rho_{\uparrow}(r),\rho_{\downarrow}(r),\nabla\rho_{\uparrow}(r),\nabla\rho_{\downarrow}(r)]. \tag{2.26}$$

The GGA has reduced the errors of LDA, but the variation of electron density still must be slow enough.

2.4 Mott Insulators

Though density functional theory successfully describes various properties of materials, there still exist some systems like Mott insulators, named after N. F. Mott, cannot be explained. In 1937, J. H. de Boer and E. J. W. Verwey indicated that a variety of transition metal oxides predicted to be conductors by band theory are insulators [8]. Also in 1937, N. F. Mott and R. Peierls tried to explain that this anomaly can be the result of that band theory did not consider the on-site electron-electron Coulomb repulsion. Since the density functional theory is a mean-field single particle theory, which cannot describe the many-bode correlations, there must be some modifications. The Hubbard model and the improved density functional theory, the so-called DFT+U, will be introduced in the following subsections.

2.4.1 Hubbard Model

The Hubbard model, originally proposed in 1963 [9, 10], is an approximate model which can be used to solve the anomaly of Mott insulators. First, we regard the nuclei in the system as the fixed array, i.e. without considering the lattice vibrations. For simplicity, every site of the array has only one energy level, thus only two electrons can occupy an energy level (spin up and spin down) due to the Pauli principle. Electrons move around the array of nuclei interact via a screened Coulomb interaction, the biggest interaction will be the Coulomb repulsion of the two electrons occupy the same site. For simplicity, There is no interaction between electrons on different sites. The on-site interactions are modeled by a term which is zero if the atom is empty of electrons or has only a single electron on it, but has the value of repulsion energy U if the atom has two electrons. The competitive term, the kinetic term, is introduced allowing electrons to move from one site to another. The energy scale t which governs this 'hopping' will

be determined by the overlap of two wavefunctions. Since wavefunctions decay exponentially, we can consider that the hopping only occurs between the neighboring atoms.

Now, we can write down the Hubbard Hamiltonian. To begin with, we recall the creation and annihilation operators which deal with the harmonic oscillator. We will spend some time reviewing their properties, which parallel those of the operators in the Hubbard model in many ways, in this more familiar setting.

$$\widehat{a} = \sqrt{\frac{m\omega}{2\hbar}}\widehat{x} + i\sqrt{\frac{1}{2m\omega\hbar}}\widehat{p} \quad and \quad \widehat{a}^{+} = \sqrt{\frac{m\omega}{2\hbar}}\widehat{x} - i\sqrt{\frac{1}{2m\omega\hbar}}\widehat{p}, \tag{2.27}$$

where $\widehat{p}$ and $\widehat{x}$ are momentum and position operators. From $[\widehat{p}, \widehat{x}] = -i\hbar$, it is easy to show that these operators obey the commutation relations,

$$\left[\widehat{a}, \widehat{a}^{+}\right] = 1, \tag{2.28}$$

and the Hamiltonian is

$$\widehat{H} = \frac{1}{2m}\widehat{p}^2 + \frac{1}{2}m\omega^2\widehat{x}^2 = \hbar\omega(\widehat{a}^{+}\widehat{a} + \frac{1}{2}). \tag{2.29}$$

The Hubbard model is also written in terms of 'fermion' creation and annihilation operators. However, there are several different respects. The fermion operators in the Hubbard model are not introduced in terms of familiar position and momentum operators. They are distinguished by attaching indices j and σ (spin up or spin down) which can be written as $\widehat{c}^{+}_{i\sigma}$ and $\widehat{c}_{i\sigma}$, where $\widehat{c}^{+}_{i\sigma}$ is the operator which creates an electron of spin σ on lattice site i, $\widehat{c}_{i\sigma}$ is the operator which annihilates an electrons of spin σ on lattice site i, and $n_{i\sigma} = \widehat{c}^{+}_{i\sigma}\widehat{c}_{i\sigma}$ is the number operator. As a consequence, the occupation number states are no longer characterized by a single number n, as for a single harmonic oscillator, but instead by a collection of occupation numbers $n_{i\sigma}$. We can write a state as $\mid n_{1\uparrow}, n_{2\downarrow}, n_{3\downarrow}, ... >$. Because these operators are used to describe fermions, they must satisfy the following relations to agree with the Pauli principle,

$$\begin{aligned} \{\widehat{c}_{i\sigma}, \widehat{c}^{+}_{j\sigma'}\} &= \delta_{i,j}\delta_{\sigma,\sigma'} \\ \{\widehat{c}^{+}_{i\sigma}, \widehat{c}^{+}_{j\sigma'}\} &= 0 \\ \{\widehat{c}_{i\sigma}, \widehat{c}_{j\sigma'}\} &= 0, \end{aligned} \tag{2.30}$$

where $\{\widehat{A}, \widehat{B}\} = \widehat{A}\widehat{B} + \widehat{B}\widehat{A}$ (the anticommutation relation). The maximum occupation of a particular site with a given spin is 1. The Hubbard Hamiltonian is then,

$$H = -t\sum_{\langle i,j\rangle\sigma}\widehat{c}^{+}_{i\sigma}\widehat{c}_{j\sigma} + U\sum_{i}\widehat{n}_{i\uparrow}\widehat{n}_{i\downarrow} - \mu\sum_{i}(\widehat{n}_{i\uparrow} + \widehat{n}_{i\downarrow}). \tag{2.31}$$

The first term is the kinetic term. It describes the annihilation of an electron of spin σ on site j and its creation on site i (or vice-versa). The symbol $<i, j>$ emphasizes that hopping is allowed

only between two neighboring sites. The second term , the correlation term, is the Coulomb repulsion energy, an energy U will be added if there is doubly occupied on j-site. The competition between the kinetic term and the correlation term characterize the system. As $t/U >> 1$, the energy is minimized making the kinetic term as small as possible through delocalization (little price is paid on the occupied atomic sites to overcome repulsion U). As $t/U << 1$, the kinetic energy of electrons is not large enough to overcome the on-site repulsion. Electrons undergo a Mott localization. The last term is a chemical potential term which controls the filling. We refer to the situation where the filling is one electron per site as 'half-filling' since the lattice contains half as many electrons as the maximum number (two per site). Studies of the Hubbard model often focus on the half-filled case because it exhibits a lot of interesting phenomena (Mott insulators, anti-ferromagnetic order, etc.)

2.4.2 Beyond DFT : DFT+U

Due to the insufficiency of density functional theory describing the strong correlated system, several attempts like the self-interaction correction (SIC) method [11], the Hartree-Fock (HF) method [12] and the GW approximation (GWA) [13] for improving the DFT were proposed. However, any of them has its inadequacy. From 1990 to 1995, the LDA+U method consists in a Hubbard-like correction to the LDA energy functional was introduced and developed by Anisimov and coworkers, which gives a better description of electronic correlations. A rotationally invariant version was introduced by Liechtenstein et al. [14], and the simplified approach was introduced by Dudarev et al. [15],

$$E_{LSDA+U} = E_{LSDA} + \frac{(U-J)}{2}\sum_{\sigma}(n_{m,\sigma} - n_{m,\sigma}^2), \tag{2.32}$$

where U and J are screened Coulomb and exchange parameters.

Chapter 3

Crystal Field Theory

Crystal Field Theory (CFT) is an ionic theory that describes the breaking of symmetries of orbital states, usually d or f-orbitals, in the presence of surrounding ligands. It was proposed by the physicist Hans Bethe in 1929 [16]. Subsequent modifications were proposed by J. H. Van Vleck [17] to allow for some covalency in the interactions to be successfully used to explain and predict some magnetic, spectral and thermodynamic properties of transition metal complexes.

3.1 Atomic Orbitals

An atomic orbital is the probability distribution of electrons around the nucleus of atom. The shape of the orbital mainly depends on the quantum numbers (n, the principle quantum number, l, the orbital quantum number, and m, the angular momentum quantum number) associated with the particular energy state. Each set of quantum numbers of an orbital can be occupied by two electrons, spin up and down, as listed in Table 3.1. To understand CFT, it is important to have

Table 3.1: Quantum numbers of atomic orbitals are listed, where n ($n \in N$) is the principle quantum number, l ($l = 0, 1, ..., n-1$) is the orbital quantum number and m ($m = 0, \pm 1, ..., \pm l$) is the angular momentum quantum number.

orbital	s	p	d	f
	l=0	l=1	l=2	l=3
n=1	m=0			
n=2	m=0	m=0, $\pm$1		
n=3	m=0	m=0, $\pm$1	m=0, $\pm$1, $\pm$2	
n=4	m=0	m=0, $\pm$1	m=0, $\pm$1, $\pm$2	m=0, $\pm$1, $\pm$2, $\pm$3

a clear picture of the shapes (angular dependence functions) of the d-orbitals. Consider a free transition metal atom. There are five d-orbitals in two spatial groups, three of the five d-orbitals (d_{xy}, d_{yz} and d_{zx}) are collectively referred to as t_{2g}, means that all three (t) orbitals have the

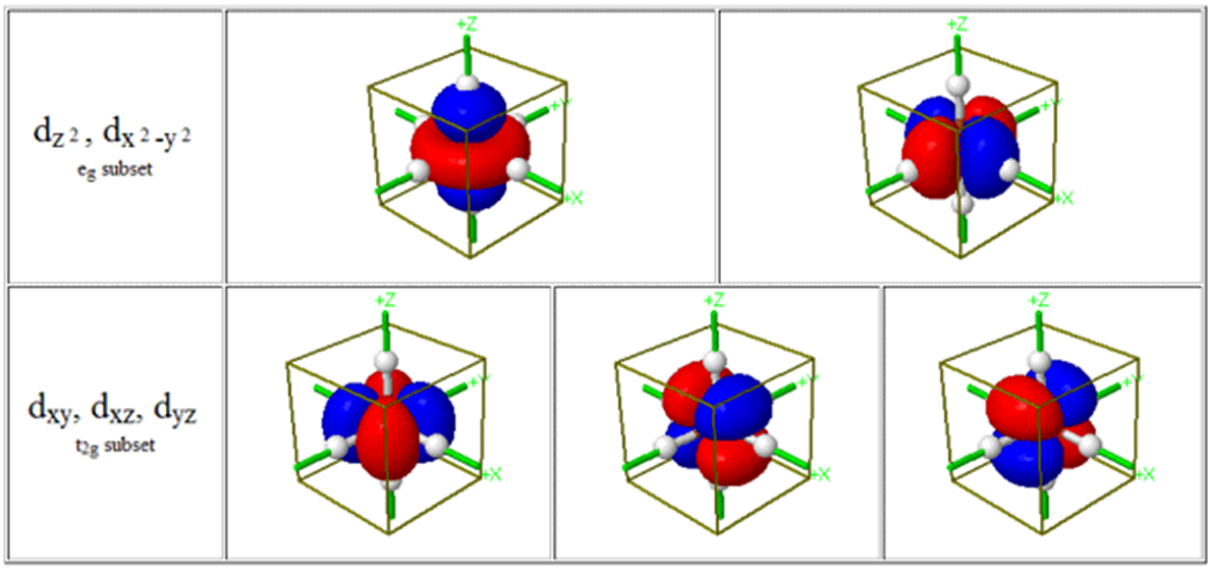

Figure 3.1: d-orbitals - For $d_{x^2-y^2}$, the four lobes lie on the x and y axes, and for d_{z^2}, there are two lobes on the z axes and there is a donut shape ring that lies on the xy-plane around the other two lobes. The four lobes of d_{xy} orbital lie in-between the x and the y axes, and so on. [Jmol: an open-source Java viewer for chemical structures in 3D. http://www.jmol.org/]

reflection asymmetry (2) and inversion symmetry (g). Take d_{xy} for example, the four lobes lie in-between the x and the y axes as can be seen in Figure 3.1, and so on. The remaining two (d_{z^2} and $d_{x^2-y^2}$) as e_g, means that both two (e) orbitals have the reflection symmetry (1) and inversion symmetry (g). For $d_{x^2-y^2}$, the four lobes lie on the x and y axes, and for d_{z^2}, there are two lobes on the z axes and there is a donut shape ring that lies on the xy-plane around the other two lobes. All d-orbitals are degenerat when the atom is free. However, in the presence of surrounding ligands, symmetries of d-orbitals are broken. Energy of t_{2g} and e_g split into two levels in octahedral and tetrahedral cases. More complex splittings occur in other cases and will be discussed in the following sections.

3.2 Crystal Field Theory

As mentioned before, CFT is an ionic theory. The ligands are regarded as point charges, the interactions between the metal ion and the ligands are purely electrostatic. All covalent bonding effects are ignored. Here we firstly look at the most common case, the octahedral complex. Six ligands attached to the central transition metal along x, y and z axes, forming an octahedron as shown in Figure 3.2. We can see that symmetries of orbitals d_{xy}, d_{yz} and d_{zx} do not change in the presence of the ligands, and remain in the t_{2g} group. Orbitals d_{z^2} and $d_{x^2-y^2}$ also remain in the e_g group. While orbitals of t_{2g} set are farther from the ligands than e_g set that lobes of orbitals directly lie along the x, y and z axes, which will have lower energy due to experience less Coulomb repulsion from ligands. Now the energy of d-orbitals of the atom split into a three-fold degenerate level and a two-fold degenerate level with an energy difference, the crystal-field

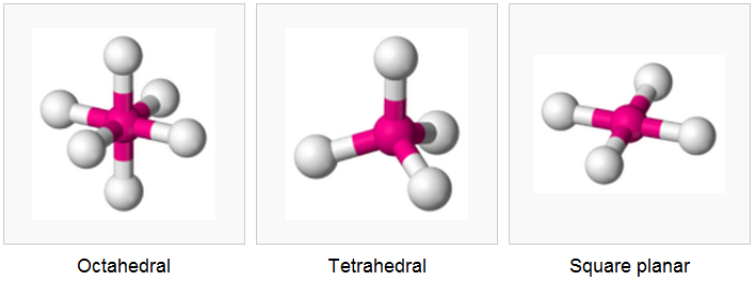

Figure 3.2: Structure of complexes - (a) The octahedral complex, where six ligands attached to the central transition metal along x, y and z axes, forming an octahedron. (b) The tetrahedral complex, four ligands form a tetrahedron around the central ion. (c) The square-planar complex, which can be seen as the simplification of the octahedral complex, where the two ligands along the z-axis are removed.

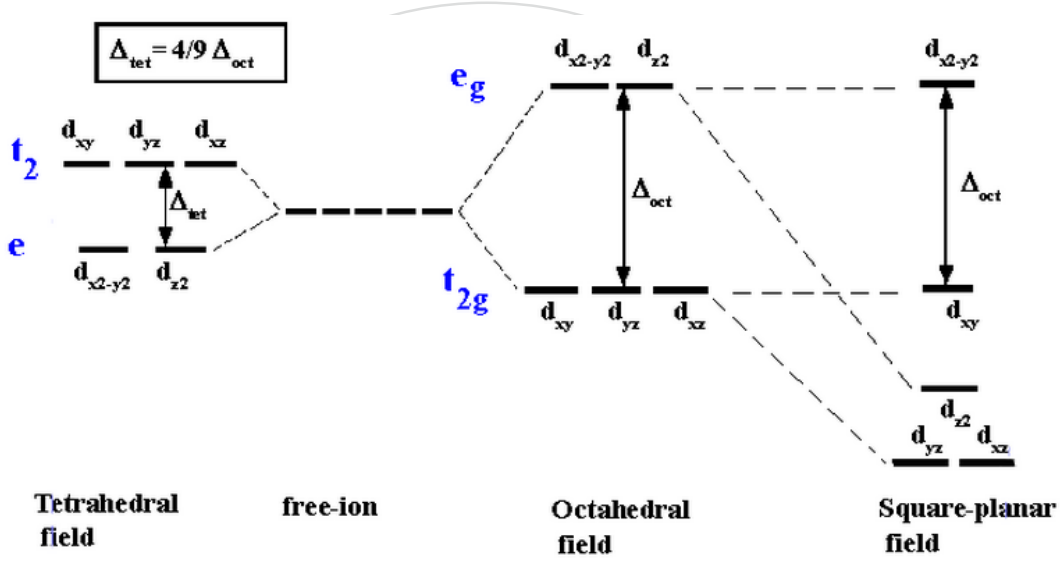

Figure 3.3: Common crystal field splittings of d-orbitals

splitting parameter (Δ_{oct}). Likewise, the other cases like tetrahedral, square-planar cases and even the more complex cases can all be discussed in the same way. As shown in Figure 3.3, in the tetrahedral case, the d-orbitals also split into two levels (t_2 and e) with energy difference (Δ_{tet}), while the more stable orbitals are d_{z^2} and $d_{x^2-y^2}$ which are oppsite to the octahedral case. And we can find that the energy difference of the tetrahedral case is smaller than the octahedral case. This is because that a tetrahedral complex has fewer ligands, and Δ_{tet} is roughly equal to 4/9 Δ_{oct}. The square planar case can be considered as an extension of the octahedral case, more complex energy levels of the d-orbitals could be obtained by discussing in the same way. Except for the arrangement of the ligands around the metal ion that can affect the splitting way of energy levels, the oxidation of the atom can dominate the magnitude of the energy splitting of the d-orbitals. A higher oxidation state of the atom leads to a larger splitting because that the ligands are closer to the atom. The nature of the ligands surrounding the metal ion also affects the magnitude of the energy splittings. The following series is the part of so-called spectrochemical

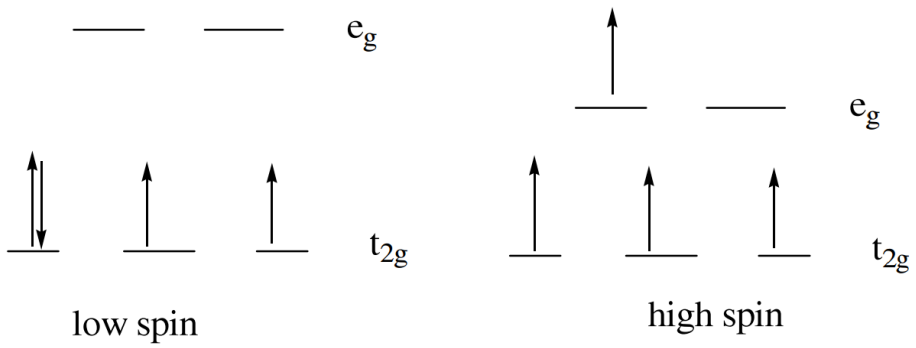

Figure 3.4: The low-spin and high-spin cases in the octahedral crystal field - In the left case, the low-spin case, the strong-field ligands lead to a large Δ_{oct}, which is larger than the pairing energy so that the lower energy orbitals will completely be filled before occupation of the higher orbitals occurs. In the right case, the high-spin case, the weak-field ligands lead to a small Δ_{oct}, which is smaller than the pairing energy so that it is easier to put the remaining electrons into the higher levels of e_g set.

series, an empirically series, the ability of ligands to lead to the splitting of energy are listed.

$$CO > CN^- > NO_2^- > NH_3 > SCN^- > H_2O > OH^- > F^- > SCN^- > Cl^- \qquad (3.1)$$

Ligands that lead to a large splitting, at the left side of the series, of energy are called strong-field ligands. Those at the right side are called weak-field ligands. Interestingly, the series above against the CFT where CO, NH_3 and H_2O are neutral ligands rather than anions, and CO is found to be one of the strongest ligands. The reasons behind this can be explained by ligand field theory (LFT), which delivers insight into the process of chemical bonding in transition metal complexes, will not be discussed here.

3.3 High Spin and Low Spin

Considering the octahedral complex, where energy split into two levels of t_{2g} and e_g sets. One may worry about how electrons occupy these orbitals. When there are four to seven electrons in the d-orbitals of the atom, two possible diagrams of distribution of electrons can occur, namely high-spin or low-spin. Take a four-electrons complex for example. The first three elections occupy the orbitals of t_{2g} set with no doubt, and the remaining one electron occupies the d-orbitals in two ways as shown in Figure 3.4. The right diagram refers to as the high-spin case. The weak-field ligands lead to a small Δ_{oct} so that it is easier to put the remaining electron into the orbitals of e_g set than put into the orbitals of t_{2g} set to form a pair. This is because that two electrons put into the same orbial would repel each other due to the Coulomb repulsion, and the energy cost is larger than Δ_{oct}. Therefore, electrons tend to occupy each of the five d-orbitals before any pairing occur in accord with Hund's rule. Conversely, a large Δ_{oct} caused by the strong-field ligands lead to the low-spin case. The remaining one electron tends to form a pair in

the orbitals of t_{2g} set because the energy cost of pairing is smaller than Δ_{oct}. The lower energy orbitals will completely be filled before occupation of the higher orbitals occurs according to the Aufbau principle. By the way, as mentioned before, the crystal field splitting energy for tetrahedral complex is refer to as Δ_{tet}, and is roughly equal to $4/9\Delta_{oct}$, which is typically small enough to tend to the high-spin case. The two diagrams can be used to explain or predict some magnetic properties of some compounds like magnetic moment and number of unpaired electrons. A compound has unpaired electrons will lead to the paramagnetic property and be attracted by magnetic field, while a compound with all electrons paired will lead to the diamagnetic property and be weakly repeled by magnetic field. By using the simple spin-only formula, we can predict the magnetic moment,

$$\mu = \sqrt{4S(S+1)}, \tag{3.2}$$

where S is the spin quantum number (1/2 for each unpaired electron) and the unit of the moment is Bohr magneton (μ_B). We can also determine the number of unpaired electrons by measuring the magnetic moment and analysing the nature of the compound.

3.4 Crystal Field Stabilization Energy

A compound in the ground state means that electrons distribute in the most stable way in the system. Any excited system tends to go through a transition to the state with the best stability. There is a parameter for counting the stability of a state of the system called crystal field stabilization energy (CFSE) in CFT. It is easy for us taking an example to discuss the so-called CFSE. For an octahedral complex, the energy levels split into the lower t_{2g} level and the higher e_g level, and the energy difference is Δ_{oct}. An electron in the more stable t_{2g} orbital is treated as contributing $-0.4\Delta_{oct}$, whereas an electron in the higher energy e_g orbital contributes to a destabilisation of $+0.6\Delta_{oct}$ to CFSE. The more stable of the state to the system, the smaller the value of CFSE. If the electron pairing (put two electrons into the same orbital) energy P is smaller than Δ_{oct}, it is the low-spin case. Conversely, it is the high-spin case.

As shown in Figure 3.4, four d-electrons occupy the t_{2g} orbitals in the low-spin case,

$$CFSE = (-0.4\Delta_{oct}) \times 4 + P = -1.6\Delta_{oct} + P. \tag{3.3}$$

For high-spin case,

$$CFSE = (-0.4\Delta_{oct}) \times 3 + 0.6\Delta_{oct} = -0.6\Delta_{oct}. \tag{3.4}$$

The use of CFSE enable us to predict or explain the structure of some complexes. In fact, structures of many d^8 complexes are square-plannar can be explained by CFSE. Also, crystal field stabilization can be applied to analyse transition-metal complexes of all geometries.

Figure 3.5: color wheel - A sample absorbs visible light of color of the specific wavelength and reflects the rest, in appears the complementary color of light. Find the color that is absorbed, then move directly across the wheel to the other side to get the complement.

3.5 Jahn-Teller Theorem

The Jahn-Teller theorem (named after Hermann Arthur Jahn and Edward Teller), also called Jahn-Teller distortion often, was published in 1937 [18]. The crystal distortion occur due to the asymmetry of distribution of electrons in the system, which mostly be observed in octahedral system. In the octahedral d^9 case (nine electrons occupy the d-orbitals), the ninth electron may occupy either d_{z^2} or $d_{x^2-y^2}$ orbitals. If it occupies the d_{z^2} orbital, there will be more Coulomb repulsion along the z-axis so that the compound tends to elongate along the z-axis. Conversely, elongation along x and y axes if the ninth electron occupies the $d_{x^2-y^2}$ orbital. Likewise, the distortion can occur theoretically in almost all cases except d^3, d^8, d^{10}, high-spin d^5 and low-spin d^6, since the distributions of electrons of these cases are symmetric. Considerable distortion are usually observed in high spin d^4 , low spin d^7 and d^9 cases, since the unpaired electron occupies the orbital of e_g set, the more Coulomb repulsion lead to the more distortion.

3.6 Colors of Transition Metal Complexes

Here we discuss the colors of some complexes that can be explained by CFT in this section. As we know, if a sample absorbs all wavelength of visible light, none reflects and reaches our eyes from that sample, it appears black. Conversely, if the sample do not absorb any wavelength of visible light, it appears white. Since the sample absorbs visible light of color of the specific wavelength and reflects the rest, in appears the complementary color of light. The color wheel shown in Figure 3.5 can demonstrate which color a sample will appear. Find the color that is absorbed, then move directly across the wheel to the other side to get the complement. For example, if the sample absorbs the red-light, it appears cyan, and if the sample absorbs the blue-light, it appears yellow. Now we get back to the subject, as mentioned before, energy of the d-orbitals of the transition metal atom will split into two or more levels in the presence of ligands. An electron occupies the lower energy d-orbital would jump to the higher unoccupied d-orbital as it absorbs light of wavelength correspond to the certain energy (the crystal field splitting).

Fortunately, the energy (the crystal field splitting) often corresponds to the visible region of the spectrum. Therefore, we can explain or predict colors of the transition metal complexes. In Table 3.2, a number of cobalt (III) complexes are listed [19], various ligands (including the strong-field

Table 3.2: Cobalt (III) complexes, colors and corresponding absorbed lights are listed.

Co^{3+} complex	absorbed light	color seen
$[CoF_6]^{3-}$	red	green
$[Co(H_2O)_6]^{3+}$	orange	blue
$[Co(NH_3)_5Cl]^{2+}$	yellow	violet
$[Co(NH_3)_5H_2O]^{3+}$	blue-green	red
$[Co(NH_3)_6]^{3+}$	blue	yellow-orange
$[Co(CN)_6]^{3-}$	ultraviolet	pale yellow

and weak-field ligands) combine with the cobalt ion and present different colors. The results agree with CFT well. Take $[Co(CN)_6]^{3-}$ for example, CN^- is a strong-field ligand so that it will lead to a large crystal-field splitting. Thus the energy an electron needs for transition must be high enough (ultraviolet light). Conversely, F^- is a weak-field ligand, which will lead to a small splitting. The energy of red light is large enough to excite the transition.

Chapter 4

Multiferroics

4.1 Introduction

Multiferroics is a material simultaneously having more than one ferroic order parameter in a phase. These parameters are ferromagnetism, ferroelectricity and ferroelasticity (Nowadays what most people mean by multiferroic material predominantly applies to the coexistence of magnetism and ferroelectricity). Some coexistent order parameters in the material has the cross coupling. Take a material involving the coexistance of ferromagnetism and ferroelectricity with cross coupling for example, it means that we can control the electric order in the system by applying a magnetic field and vice versa. This behavior is called the magnetoelectric effect [20]. Such material has the potential of technological applications that it provides opportinities for designing the better electronic devices in the future. As is known, the common data storage device like the hard disk drive is devised using the ferromagnetism of the material. And also the common data storage device, the flash memory, devised using the ferroelectricity of the material. The two storage devices have their respective pros and cons. If the cross coupling of a discovered multiferroic material can be strong enough, the large degrees of freedom of its properties can probably be used to devise some better electronic devices including the advantages of both hardisk and flash memory, or to create some multifunctional electronic components like a new types of 4-state logic (i.e., with both up and down polarization and up and down magnetization).

The studies of multiferroic material can be traced back to 1960s [21]. However, it has been considered that the strong enough coupling between ferromagnetism and ferroelectricity is impossible. The early studies represent that the conditions to cause the ferromagnetism and ferroelectricity usually interfere each other. For example, a condition for causing ferroelectricity requires empty d-orbitals (diamagnetic ions), while a condition for ferromagnetism requires partially filled d-orbitals (paramagnetic ions). Therefore, the interesting field has been forgotten for a while. Since the precursory works on thin films of $BiFeO_3$ [22], $TbMnO_3$ [24] and $TbMn_2O_5$ [23] in 2003, multiferroic materials attract much attention once again. Considerable effort has been devoted to search for new compounds with good multiferroic properties and even strong

enough magnetoelectric coupling. The advancements of the *ab initio* calculation and experimental techniques make it possible to predict or design the system, and to realize the mechanics of the coexistence of the order parameters and the cross coupling of them.

There are generally two types of the multiferroic materials distinguished by considering the microscopic source of the ferroelectricity. The first type, called the type-I multiferroics, contains those materials with weak or no cross coupling of ferromagnetism and ferroelectricity. Conversely, the type-II multiferroics appears the strong cross coupling between ferromagnetism and ferroelectricity. The two types of multiferroics will be discussed in the following.

4.2 Symmetry

Symmetry, has been generalized to mean invariance in physics, is that the state remain invariant after undergoing a transformation. This definition can be applied to not only concrete but also abstractive problems. Here we only treat the perspective of physics, including aspects of space and time. The behavior under spatial and time version can characterize orders in the system, since ferroelectricity, ferromagnetism and ferroelasticity are closely related to the breaking of the spatial or time inversion symmetry.

Time reversal

Time reversal is that we replace the expression for time with its negative in formulas or equations. It does not mean that we really turn back the clock, but reverse the motions. For example, an electron doing the circular motion around the z-axis clockwise, the centripetal force acting on the electron point to the center of the circle, and the magnetic field is induced along the positive z-axis. Now we have a time reversal transformation on the electron, the circular motion become counterclockwise, the centripetal force acting on the electron still point to the center of the circle. However, the magnetic field is induced along the oppsite direction, the negative z-axis. We can say that the classical mechanism of the circular motion of an electron agree with the time inversion symmetry. However, the magnetic field induced by an electron requires the breaking of time reversal symmetry. Also, the condition for ferromagnetism requires the spontaneous breaking of time reversal symmetry.

Spatial reversal

Likewise, spatial reversal is that we replace the expression for position with its negative in formulas or equations, which we also call the parity transformation. Considering a neutral atom, the symmetric center is located at the nucleus. The system without any perturbation agrees with the spatial inversion symmetry. When putting the atom in an electric field, the distribution of electrons in the surroundings of the nucleus deviate along the oppsite direction of the electric field. The breaking of the spatial inversion symmetry occurs producing an electric polarization in

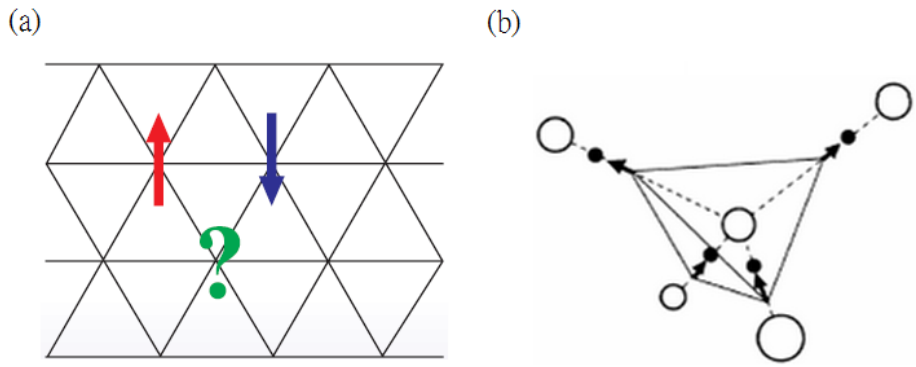

Figure 4.1: Geometric frustration - (a) Ising antiferromagnets on the triangle lattice. The remaining one spin can no longer point in a direction oppsite to both two spins. (b) Scheme of water ice molecules where hollow circles are oxygen atoms and filles circles are hydrogen atoms. For each oxygen atom, two of the neighboring must reside in the far position and two of them in the near position.

the atom. The condition for ferroelectricity requires the spontaneous breaking of spatial reversal symmetry.

4.3 Geometric Frustration

The concept of geometric frustration [25, 26] is important in some system. It means that there is no single ground state in the system. A nonzero entropy remains in the system even at zero temperature. It can be traced back to 1950 [27]. An Ising antiferromagnet on the triangle lattice, when two of three spins are pointed in oppsite directions to satisfy their antiferromagnetic interaction, the remaining one can no longer point in a direction oppsite to both two spins. That is to say, it is impossible to simultaneously minimize the energy of all interactions. The geometric frustration is not a phenomenon occurs unusually. In fact, it occurs in the ordinary ice which we contact almost everyday [28]. Four oxygen atoms form a tetrahedral structure, and the hydrogen atoms locate between two oxygen atoms being closer to one of the two. Every oxygen atom is surrounded by four hydrogen atoms. For each oxygen atom, two of the neighboring must reside in the far position and two of them in the near position, so-called 'Ice rules'.

4.4 Multiferroics

4.4.1 Type-I Multiferroics

The sources of ferromagnetism and ferroelectricity of type-I multiferroic materials are different, and weak or no magnetoelectric effect appears in such a system. The critical temperature of appearance of ferroelectricity is often higher than magnetism, and the spontaneous electric polarization P (of order 10 - 100 μC/cm^2) is often rather large. Four different subclasses de-

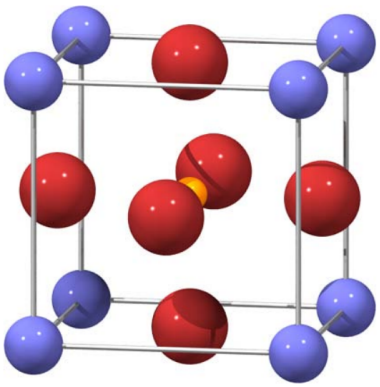

Figure 4.2: Perovskite Structure - The general stoichiometry ABX_3, where A (blue particles located at the corners of the cube) and B (orange particle located in the centre of the cube) are cations and X (red particles located in the face-centred positions of the cube) are anions.

pending on the mechanism of ferroelectricity will be discussed as follows.

Perovskites

Firstly, we introduce the perovskite structure which has the general chemical formula ABX_3, named originating from the perovskite mineral ($CaTiO_3$), where A and B are cations and X is an anion (often the oxygen atom). In an ideal perovskite structure, the A cations (blue) is located at the corners of the cube, the B cations (orange) in the centre and the X anions (red) in the face-centred positions. There are many magnetic and ferroelectric materials with the perovskite structure. What scientists want to find is a material simultaneously has the ferromagnetism and ferroelectricity with strong cross coupling. But, early studies represent that the conditions to cause the ferromagnetism and ferroelectricity usually interfere each other. For example, a condition for causing ferroelectricity requires empty d-orbitals, while for ferromagnetism requires partially filled d-orbitals. It is considered that the coexistence of ferromagnetism and ferroelectricity is impossible. However, out of speculation, some materials with perovskite structure do simultaneously have the ferromagnetism and ferroelectricity [29, 30], for example, $RMnO_3$ (R=Tb, Dy, Ho). This is the so-called d^0-d^n problem. A possible way to explain this problem is to make "mixed" perovskite with d^0 and d^n ions. It means that the source of the ferromagnetism and ferroelectricity originate from different ions. The d^0 transition metal ions locate on B-cites, the empty d-orbitals hybridized with p-orbitals of the surrounding one or three oxygen atoms forming the strong covalent bond and causing the off-centered shifts which break the spatial inversion symmetry, i.e. causing the spontaneous electric polarization. And the d^n ions locate on A-cites contributing to the ferromagnetism. There seens to be no contradiction in this way. Unfortunately, this kind of multiferroic materials have weak or no cross coupling between ferromagnetism and ferroelectricity since the sources are different.

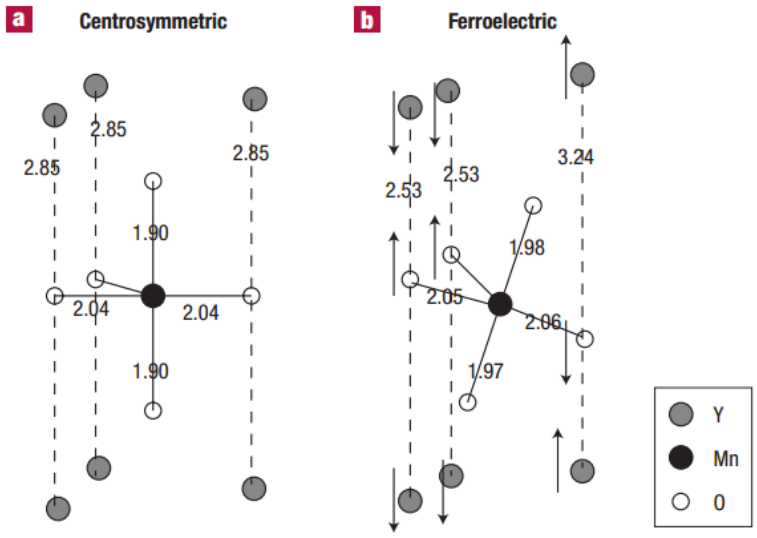

Figure 4.3: $YMnO_3$ - (a) The centrosymmetric structure above the critical temperature. (b) The ferroelectric structure below the critical temperature where practically rigid MnO_5 tilt breaking the spatial inversion symmetry.

Lone Pairs

There is another way oppsite to the above one to explain the coexistence of ferromagnetism and ferroelectricity, where ferroelectricity is caused by the A-cite cations, and the B-cite cations contribute to the ferromagnetism. This way usually occurs on those materials with perovskite structure having active ns^2 electrons, called lone-pair, on the cations located on A-cite. Take $BiFeO_3$ for example, the outer Bi-$6s_2$ lone-pair cause the empty Bi-$6p$-orbital to come closer in energy to the O-$2p$-orbital. This lead to the hybridization of Bi-$6p$ and O-$2p$ orbitals and drive the off-centered shifts resulting in the ferroelectricity. And the d^n transition metal ions locate on B-cites contributing to the ferromagnetism. No contradiction occurs. However, the magneto-electric effect in this kind of system is none or weak, due to different sources of ferromagnetism and ferroelectricity.

Structured Distortion

The mentioned two above are related to bondings that lead to the off-centered shifts of atoms. Here we introduce a mechanism of ferroelectricity caused by the relatively complicated deformation of the crystal structure. Take $YMnO_3$ [32]for example, a tilting of the practically rigid MnO_5 in the crystal occurs as belowing the critical temperature. The asymmetric change of distance of Y-O bonds in the system lead to the ferroelectricity. And the ferromagnetism comes from the magnetic Mn^{3+} ions.

Charge Ordering

In the typical ferroelectric materials, the main source of ferroelectricity is the deformation of cations and anions in the crystal as above. Recently, it is found that the ferroelectricity can occur due to the charge ordering [31]. In some strong correlation systems, due to the strong interaction between electrons, charges are localized on different sites leading to a disproportion and an ordered superlattice breaking the spatial inversion symmetry. This is often observed in transition metal oxides, especially those formally containing transition metal ions with different valence. For example, the magnetite Fe_3O_4 is a mixed-valence oxide where the iron atoms have a statistical distribution of Fe^{3+} and Fe^{2+} above the critical temperature. Below the critical temperature, the combination of Fe^{2+} and Fe^{3+} species arrange themselves in an ordering pattern, causing the ferroelectricity.

4.4.2 Type-II Multiferroics

The theme of multiferroics which gets the most attention recently is the type-II multiferroics. The discovery of strong magnetoelectric effect in the materials excite scientists to devote rather considerable effort to search for new compounds and theoretical models. They can be separated into two groups with different mechanisms of multiferroics, the spiral and collinear magnetic structures in the materials as follows.

Spiral Magnetic Structure

The first group is the spiral magnetic structure in the material which appears below the critical temperature along with the ferroelectricity. Most of the type-II multiferroics known to date belong to this group. Take the pioneering work on $TbMnO_3$ for example [24]. Below T_{N1}, the magnetic structure is a sinusoidal spin-density wave, and every spins point to the same direction but different magnitude of local moment. The magnitude of these moments varies periodically as shown in Figure 4.4 [33]. This structure is centrosymmetic and consequently not ferroelectric. As the temperature decreases below T_{N2}, the cycloidal spiral with the wave vector $\mathbf{Q} = \mathbf{Q}_x$ and spins rotating in the xz-plane appears. The spontaneous electric polarization along the z-axis appears since the spiral magnetic structure break the spatial inversion symmetry. By applying the strong enough magnetic field along the y-axis, the direction of electric polarization will change from z-direction to x-direction. The strong magnetoelectric effect inspire scientists to find more new compounds and study the theoretical models. A microscopic approach [34] and a phenomenological approach [35] are proposed to describe the mechanism of the electric polarization. The former, which is the so-called inverse effect of (relativistic) Dzyaloshinskii-Moriya interaction, gives a relation between the ferroelectricity and the arrangement of spins,

$$P \propto r_{ij} \times [S_i \times S_j], \tag{4.1}$$

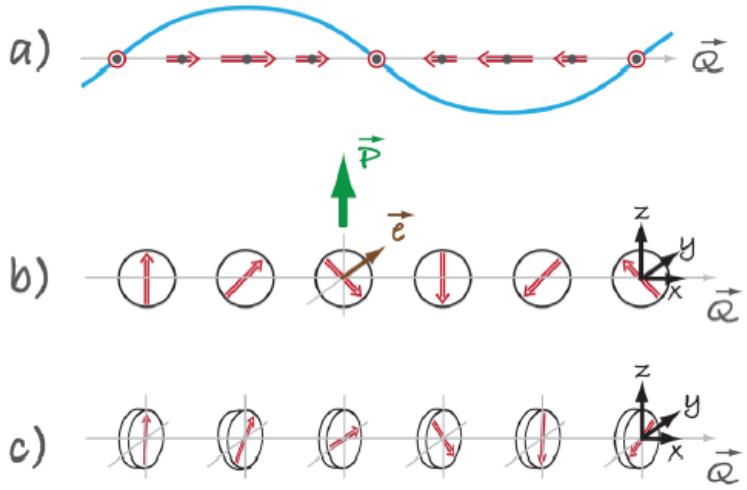

Figure 4.4: Different types of spin structures relevant for $TbMnO_3$ - (a) $T_{N2} < T < T_{N1}$. Sinusoidal spin density wave. Every spins point to the same direction but different magnitude of local moment. The magnitude of these moments vary periodically. This structure is centrosymmetic and consequently not ferroelectric. (b) $T < T_{N2}$. The cycloidal spiral magnetic structure with the wave vector $\mathbf{Q} = \mathbf{Q}_x$ and spins rotating in the xz-plane. This structure breaks the spatial inversion symmetry so that the spontaneous electric polarization appears. (c) In a so-called "proper screw" the spins rotate in a plane perpendicular to $\mathbf{Q}$. Here the inversion symmetry is broken, but most often it does not produce polarization.

where r_{ij} is the vector pointing from spins S_i to S_j. The magnitude of the polarization is proportional to the spin-orbit coupling constant. In a particular case, the spiral magnetic structure as shown in Figure 4.4(c) breaks the spatial inversion symmetry but appears no ferroelectricity most often, although in certain cases it might. And the later also gives a relation obtained by analysing the symmetries of the ferroelectricity and the magnetism of the system,

$$P \propto [(M \cdot \nabla)M - M(\nabla \cdot M)]. \tag{4.2}$$

Since the ferroelectricity occurs relating to the magnetism, it is not surprised that the ferroelectricity is strongly affected by the magnetic field.

Collinear Magnetic Structure

In the second group, the collinear magnetic structure in the material strongly affects the ferroelectricity. All spin moments aligned along the same direction, and the spin-orbit coupling in the system is neglected. Since the strength of exchange striction of ferromagnetic and antiferromagnetic arrangements of two neighbor spins ($\uparrow\uparrow$ and $\downarrow\downarrow$) are different, the crystal distortion may occur breaking the spatial inversion symmetry, i.e. lead to the spontaneous electric polarization. When the magnetic field is applied in the certain direction, direction of the electric polarization changed relating to the transformation of spin arrangement. Take Ca_3CoMnO_6 for example, the crystal has the inversion symmetry at high temperature. However, below the crit-

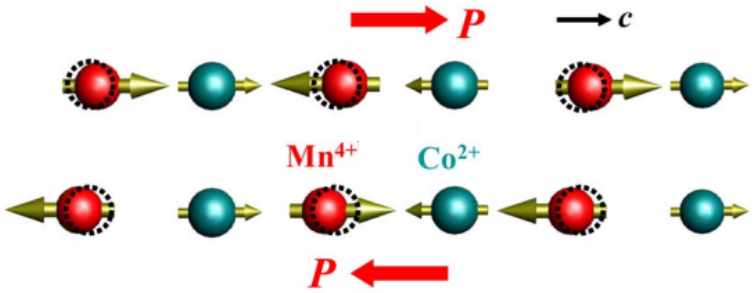

Figure 4.5: Ising chain composed of Co^{2+} and Mn^{4+} - Ising chains with the up-up-down-down spin order and alternating ionic order, in which electric polarization is induced through symmetric exchange striction. The two possible magnetic configurations leading to the opposite polarizations are shown. The atomic positions in the undistorted chains are shown with dashed circles.

ical temperature, Co^{2+} and Mn^{4+} ions alternating along the simplified Ising chains exhibit an up-up-down-down ($\uparrow\uparrow\downarrow\downarrow$) magnetic order. Two possible crystal distortion due to the exchange striction are shown in Figure 4.5. The two possible magnetic configurations leading to the opposite polarizations are shown. In this case, valences of the two transition metal ions are different (Co^{2+} and Mn^{4+}), and thus lead to the different strength of exchange striction. Interestingly, the same effect occur even for same magnetic ions despite the fact that the exchange interaction in transition metal oxides usually occurs via intermediate oxygens and depends on both the distance between the metal ions and the metal-oxygen-metal bond angle.

Chapter 5

Calculated Physical Properties of $Cu_3Mo_2O_9$

5.1 Introduction

The magnetoelectric multiferroics [36] is the material which involve the coexistance of magnetic and electric order with cross coupling. It means that we can control the electric order in the system by applying a magnetic field and vice versa, i.e., the so-called magnetoelectric effect [20]. Such materials provide opportunities for devising the multifunctional electronic devices in the future. However, it has been considered that strong enough coupling between magnetic and electric order is impossible in 1960s, and hence such interesting field has been forgotten for a while. Since the precursory work on $TbMnO_3$ [24], multiferroics attracted much attention once again. Considerable effort has been devoted to search for new compounds with strong magnetoelectric coupling. Recently, an interesting material $Cu_3Mo_2O_9$ has been found by Kuroe et al. [37] that it has remarkable magnetoelectric effect being as strong as $TbMnO_3$. What is the most special is that the origin of the electricity of this material probably be a novel mechanism. A small spin cluster model has been suggest by Kuroe et al. which is very different from the magnetic superlattice. Such interesting system motivated us to have some theoretical simulations to study it.

$Cu_3Mo_2O_9$ was prepared as a brown-orange powder by Vilminot et al. [38], and the space group is orthorhombic Pnma measured using X-ray powder diffraction. There are three crystallographically inequivalent Cu sites (Cu1, Cu2 and Cu3) as shown in Figure 5.1 [39]. The quasi-one-dimensional chains formed by Cu_4 tetrahedra are connected by bridging MoO_4 which is not presented in the figure for simplifying, and each two neighboring Cu atoms are bridged by an oxygen ion. Four formular unit (f.u.) are included in a primitive unit cell. The magnetism is dominated by Cu ions, each has spin $\frac{1}{2}$, while other ions are nonmagnetic. Since each Cu chain is a segment of the pyrochlore structure, geometric frustration possibly plays an important role in this system, i.e. the system has degenerate ground states. Therefore, the magnetic struc-

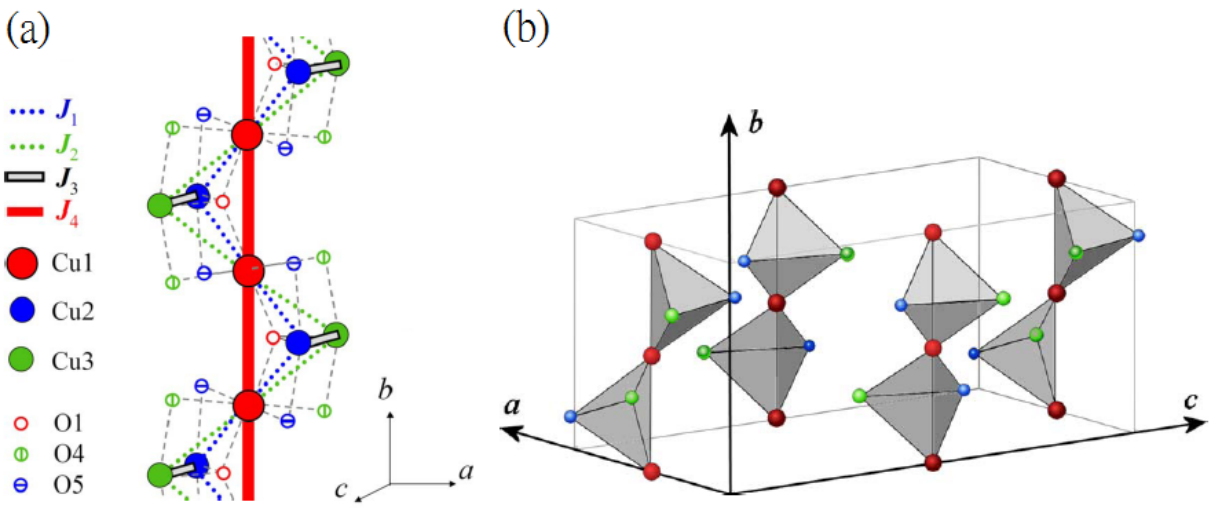

Figure 5.1: Structure of $Cu_3Mo_2O_9$ - (a) Three crystallographically inequivalent Cu^{2+} sites (Cu1, Cu2 and Cu3) are included in the system. The quasi-one-dimensional chain is formed by Cu_4 tetrahedra, and each two neighboring Cu atoms are bridged by an oxygen ion. (b) The quasi-one-dimensional chains are connected by bridging MoO_4 which is not drawn in the figure for simplifying. Four formular units (f.u.) are included in a primitive unit cell.

ture cannot be completely defined easily. There are experiments trying to infer some guessed magnetic configurations which agree with their experimental results. For example, the symmetric analysis of the neutron diffraction experiments [38] gave a guessed spin configuration with all spins lying on the *ac*-plain as shown in Figure 5.2 (a). Only spins on Cu1 and Cu3 are presented. Another example is a series of experiments performed by Hamasaki et al. [39]. A weak-ferromagnetic phase below $T_c \simeq 2.5$K and an antiferromagnetic phase below $T_N = 7.9$K are determined. A guessed spin configuration was suggested as shown in Figure 5.2 (b). Only spins on Cu1 are presented, pointing almost along the *b*-axis and being canted by the DM interaction. Spins on Cu2 and Cu3 are considered forming singlet dimers which weakly interact with Cu1 on the antiferromagnetic chains. We can see that the two guessed of spin configurations are very different. The magnetic structure in the system has not been determined. The spontaneous electric polarization density below T_N apperas along *c*-axis ($P_{\|c} \simeq 500\ \mu C/m^2$). The magnitude is close to that of $TbMnO_3$. When applying the magnetic field along *c*-axis, the direction of the electric polarization switches to the *a*-axis ($P_{\|a} \simeq 800\ \mu C/m^2$) as shown in Figure 5.3 [37]. The most interesting point is that Kuroe et al. suggest a small spin cluster model to be the source of the ferroelectricity, which is very different from the spin superlattice in $TbMnO_3$.

Since the magnetic structure and the origin of electricity have not been clarified yet, and there still is no *ab initio* study of $Cu_3Mo_2O_9$, here we perform electronic structure calculations to study its magnetic structure and also the electric polarization.

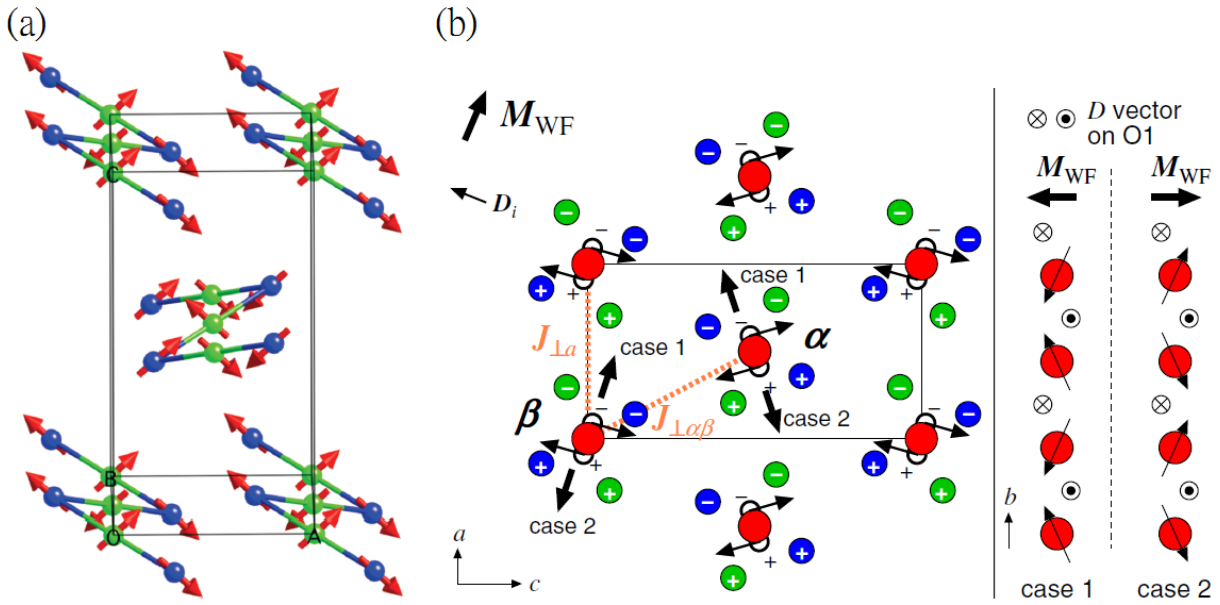

Figure 5.2: Guessed spin configurations - (a) The symmetric analysis of the neutron diffraction experiments gave a guessed spin configuration with all spins lying on the *ac*-plain. Only spins on Cu1 and Cu3 are presented. (b) Hamasaki et al. suggested a rather different spins configuration. Only spins on Cu1 are presented, pointing almost along the *b*-axis and being canted by the DM interaction. While spins on Cu2 and Cu3 are considered forming singlet dimers which weakly interact with Cu1 on the antiferromagnetic chains.

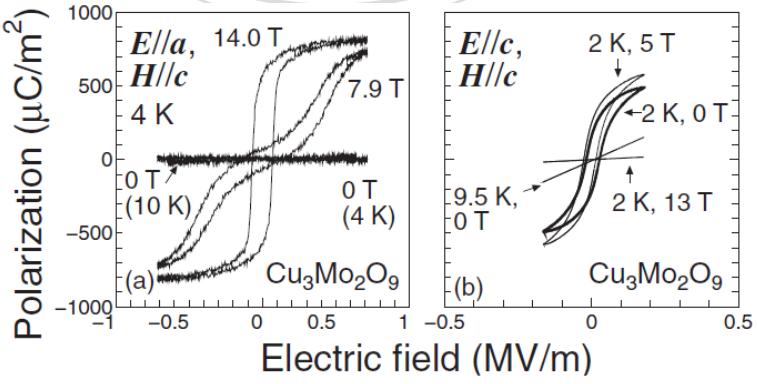

Figure 5.3: Ferroelectricity of $Cu_3Mo_2O_9$ - The spontaneous electric polarization apperrs along *c*-axis ($P_{\|c}$≃500 $\mu C/m^2$). When applying the magnetic field along *c*-axis, the direction of the electric polarization changes to the *a*-axis ($P_{\|a}$≃800 $\mu C/m^2$).

5.2 Crystal Structure and Computational Details

Our *ab initio* calculations are based on spin density functional theory with generalized gradient approximation (GGA). We used the accurate full-potential projector augmented-wave (PAW) method, as implemented in the VASP code. The core radii of the copper, molybdenum and oxygen atoms are 1.312 $\AA$, 1.455 $\AA$ and 0.82 $\AA$, respectively. A cut-off energy of 450 eV for plane wave expansion is used. The criterion for the convergence of the electronic selfconsistency cycles is 10^{-4} eV. The Γ-centered Monkhorst-Pack k-meshes of $6\times7\times3$ are used for Brillouin zone integration. We used the atomic structure data from the XRD experiments. There are three crystallographically inequivalent Cu sites (Cu1, Cu2 and Cu3) and seven crystallographically inequivalent O sites (O1, O2, ..., O7) as shown in Figure 5.4. Two crystallographically inequivalent Mo sites are not emphasized. We can see that each Cu ion is surrounded by O ions causing the square-planar-like crystal field. Since we consider that those O ions far away (larger than 2.15 $\AA$) from the Cu ion contribute relatively small effect and almost can be neglected. Take Cu1 and its surrounding O ions for example, the distance between Cu1 and O1 (O2, O3) ions is 1.86 (2.3, 2.13) $\AA$, the contributions of O2 ions affecting on Cu1 can be neglected. O1 and O3 ions surrounding the Cu1 ion form a parallelogram, causing the square-planar-like crystal field.

To begin with, we performed both non-magnetic (NM) and collinear spin-polarized, both ferromagnetic (FM) and anti-ferromagnetic (AFM), calculations of $Cu_3Mo_2O_9$. The results are presented in Table 5.1 (a). We found that the AFM spin configuration is the most stable one. Spins on Cu1 align an AFM chain itself, spins on Cu2 and Cu3 form a singlet dimer, i.e. spins on Cu2 and Cu3 point to oppsite directions. We also tried to find if there is a AFM spin configuration that spins on Cu2 and Cu3 form a triplet dimer, but failed. From Table 5.1 (a), both energy (meV/unit cell) and spin moments on Cu atoms (μ_B) are shown. We can see that all spin moments on Cu are small. Especially in the FM case, the moments are smaller than 0.1 μ_B on Cu1. Though it increases to be larger than 0.3 μ_B in the AFM case, it is still much smaller than the theoretical value 1.0 μ_B. In NM state, there is no energy gap. When considering the spin-polarization, energy levels of spin up and down split due to the exchange interaction, but still no gap opened in the FM state. In the AFM case, since energy levels of spin up and down split further, an energy gap 0.2 eV opens, but is still not wide enough. Since $Cu_3Mo_2O_9$ was prepared as a brown-orange powder by Vilminot et al., the absorbed energy corresponding to the complementary color of visible light must be at least 1.0 eV, i.e. the energy gap must be at least 1.0 eV. Though results of neutron diffraction experiments suggest that the magnetic structure of $Cu_3Mo_2O_9$ probably be non-collinear, rather than our collinear spin-polarized calculations here, the effects of exchange interaction are still insufficient to open a wide enough gap. We can conclude that the system must be a strong correlation system, i.e., the on-site electron-electron Coulomb interaction must be considered.

Though non-collinear spin-polarized calculations without considering the electron-electron correlations cannot give a reasonable energy gap, we still did them for conparison. The results

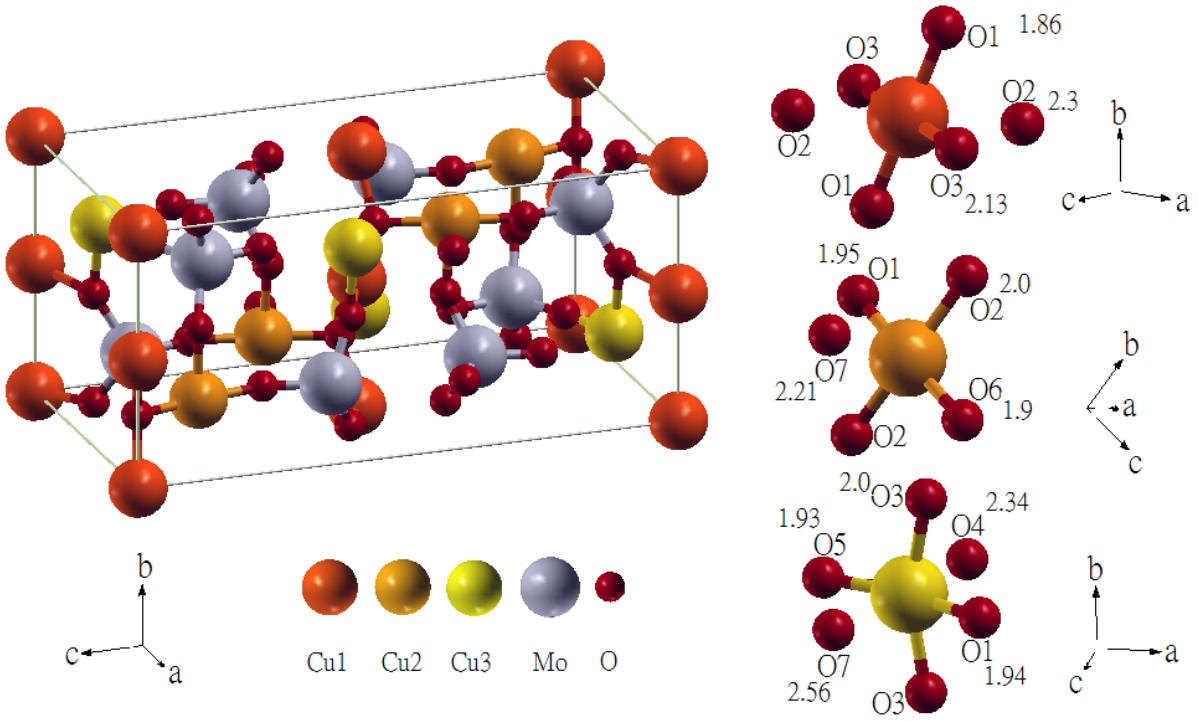

Figure 5.4: Crystal Structure of $Cu_3Mo_2O_9$ - We used the atomic structure data from XRD experiments. Their are three crystallographically inequivalent Cu sites (Cu1, Cu2 and Cu3) and seven crystallographically inequivalent O sites (O1, O2, ..., O7). Each Cu ion is surrounded by O ions causing the square-planar-like crystal field. Take Cu1 and its surrounding O ions for example, the distance between Cu1 and O1 (O2, O3) ions is 1.86 (2.3, 2.13) $\AA$. The contributions of O2 ions affecting on Cu1 can be neglected. O1 and O3 ions surrounding the Cu1 ions form a parallelogram, causing the square-planar-like crystal field.

Table 5.1: Results of NM and collinear spin-polarized (including FM and AFM) calculations are given. Energy (meV/unit cell), band gap (eV) and spin moments (μ_B) on Cu ions are listed. The electron-electron correlations have not been considered in (a) and have been considered in (b).

	(a)			(b)		
	NM	FM	AFM	FM	AFM-s	AFM-t
energy	693.5	196.59	0	273.52	0	11.68
gap	none	none	0.2	0.92	1.472	1.41
Cu1-1		0.075	-0.324	0.701	0.631	0.630
Cu1-2		0.067	0.323	0.702	0.631	0.630
Cu1-3		0.067	0.323	0.702	-0.631	-0.630
Cu1-4		0.074	-0.324	0.701	-0.631	-0.630
Cu2-1		0.549	-0.49	0.665	-0.648	-0.657
Cu2-2		0.549	-0.49	0.665	0.648	0.657
Cu2-3		0.549	0.491	0.665	-0.648	-0.657
Cu2-4		0.549	0.49	0.665	0.648	0.657
Cu3-1		0.570	0.501	0.686	0.667	-0.674
Cu3-2		0.568	0.502	0.685	-0.667	0.674
Cu3-3		0.568	-0.502	0.685	0.667	-0.674
Cu3-4		0.570	-0.502	0.686	-0.667	0.674

are listed in Table 5.2 so that those who are interested in this interesting material can compare their data with ours. As can be seen in Table 5.2 (a) and (b), two spin configurations were obtained without considering the spin-orbit coupling. Spins roughly point along the a-axis forming a ferrimagnetic as shown in (a), and spins completely point along the a-axis forming a collinear AFM configurations as shown in (b). The ferrimagnetic one reveals a metallic state, and the energy gap (0.18 eV) opened in the more stable collinear AFM one. Spin moments on Cu atoms are very small, especially on Cu1 atoms. We then took results in Table 5.2 (a) and (b) as initial settings to have calculations considering the spin-orbit coupling. The collinear AFM one converged to a similar spin configuration (Table 5.2 (d)). The spins on Cu slightly point away from the a-axis (especially on Cu2), and the gap increases slightly to 0.19 eV, while the FM one converged to completely different spin configurations (Table 5.2 (c)). Then, we performed the collinear calculations considering the electrons correlations, i.e. with generalized gradient approximation plus Hubbard U. An energy gap of 0.92 eV opens in the FM case in Table 5.1 (b), being close to the reasonable value, and all spins are aligned parallell. Spin moments increase to about 0.7 μ_B, as expected. In the AFM-t state in Table 5.1 (b), we obtained an energy gap of 1.41 eV, which agrees with our expectation. Spins on Cu1 align an AFM chain itself. Spins on Cu2 and Cu3 form triplet dimers. And in the AFM-s state, the energy gap increases further to 1.472 eV. Spins on Cu2 and Cu3 form singlet dimers. We found that the energy difference between FM and AFM cases increases after considering the electrons correlations. In the following sections, the on-site Coulomb repulsion is considered in all calculations with the commonly used values

Table 5.2: Non-collinear spin-polarized calculations without considering the Hubbard U. Energy (meV/unit cell), band gap (eV) and spin moments (μ_B) on Cu ions are given. Spin-orbit coupling is not considered in (a) and (b). Let (a) and (b) as initial settings, (c) and (d) were obtained considering the spin-orbit coupling.

	(a)			(b)		
energy	234.17			0		
band gap	none			0.18		
Cu1-1	-0.106	0.008	-0.005	-0.126	0	0
Cu1-2	-0.136	0.004	-0.003	-0.12	0	0
Cu1-3	0.042	-0.01	0.007	0.126	0	0
Cu1-4	-0.131	0.003	-0.006	0.118	0	0
Cu2-1	0.126	-0.037	-0.019	-0.529	0	0
Cu2-2	0.516	0.034	-0.025	0.53	0	0
Cu2-3	0.512	-0.043	0.028	-0.53	0	0
Cu2-4	0.441	0.002	0.026	0.531	0	0
Cu3-1	0.498	-0.009	0.018	-0.517	0	0
Cu3-2	0.547	0.015	-0.015	0.517	0	0
Cu3-3	0.548	-0.018	0.017	-0.518	0	0
Cu3-4	0.514	-0.003	0.006	0.518	0	0

	(c)			(d)		
energy	188.21			0		
gap	none			0.19		
Cu1-1	0.008	0.005	-0.013	-0.073	-0.004	-0.003
Cu1-2	0.037	0.047	-0.008	-0.077	0.004	0.004
Cu1-3	0.008	-0.005	0.013	0.073	-0.004	0.003
Cu1-4	0.117	-0.045	0.008	0.077	0.004	-0.004
Cu2-1	0.541	0.005	-0.041	-0.517	-0.001	0.098
Cu2-2	0.484	-0.013	-0.193	0.518	0.001	0.094
Cu2-3	0.522	0.021	-0.049	-0.518	0.001	-0.094
Cu2-4	0.537	-0.009	-0.073	0.517	-0.002	-0.098
Cu3-1	0.566	-0.008	0.060	-0.510	-0.004	-0.037
Cu3-2	0.552	0.001	0.082	0.510	0.004	-0.038
Cu3-3	0.549	-0.007	0.090	-0.510	0.004	0.038
Cu3-4	0.567	-0.001	0.049	0.510	-0.004	0.037

of $U = 4.5$ eV and $J = 0.9$ eV so that the reasonable band gap could be obtained.

5.3 Magnetic Structure

To begin with, we found that in the collinear FM, AFM-s and AFM-t spin configurations, all spins completely point along the *c*-axis (without considering the spin-orbit coupling) as shown in Table 5.3 (a). The AFM-s state is the most stable state and has a largest gap of 1.472 eV. When considering the spin-orbit coupling, all of them converge to similar configurations (Table 5.3 (b)) that the canting of spins away from the *c*-axis occur, especially the *b*-component of spins on Cu1, and the FM state has relatively large canting than AFM-s amd AFM-t states. As is mentioned before, the magnetic structure of $Cu_3Mo_2O_9$ is still not well understood. Two different guessed noncollinear AFM spin configurations are suggested [38, 39]. We began our calculations without considering the relativistic effect by consulting the results of neutron diffraction experiments [38] which give the guessed spin moments on Cu1 and Cu3. We also considered the suggestion of Hamasaki et al. that spins on Cu2 and Cu3 form singlet dimers. The noncollinear AFM spin configurations we found which are slightly unstable than the collinear AFM-s state (Table 5.3(a)) are similar to the results of neutron diffraction experiments. All spins lie in the *ac*-plane. The spins on Cu1 form the AFM chain along the *b*-axis, and the spins on Cu2 and Cu3 form singlet dimers as shown in Figure 5.5. We rotated the spins on Cu1 around the *b*-axis, while spins on Cu2 and Cu3 remain almost fixed. The relation between the energy and θ of spins on Cu1 in the system is displayed in Figure 5.6. The sinusoidal relation appears. We found that the most stable noncollinear AFM spin configuration in our calculations is that of angle $\theta = 107^\circ$ or 287° approximately between a-axis and direction of spins of Cu1 appear, while spins on Cu2 and Cu3 remain unchanged. As we consider the relativistic effect, all spins still lie nearly in the *ac*-plane in the most stable noncollinear AFM spin configuration. However, when spins on Cu1 rotating to another angle, the spins cant away from the *ac*-plane occur, especially on Cu1. The relation of ratio of spins along *b*-axis on Cu1 and θ of the spins on Cu1 in the system is pictured in Figure 5.7.

5.4 Exchange Interactions

To discuss the magnetic properties of $Cu_3Mo_2O_9$, we simplified the system to the effective Heisenberg model neglecting the Zeeman energy, i.e. do not considering the external field,

$$H_{eff} = -\frac{1}{2}\sum_k J_k e_i \cdot e_j, \tag{5.1}$$

where J_k is the parameter of the exchange interaction between Cu_i and Cu_j atoms, and e_i is an unit vector along the direction of local spin moment on Cu_i atom. A negative exchange

Table 5.3: Non-collinear spin-polarized GGA+U calculations. Energy (meV/unit cell), band gap (eV) and spin moments (μ_B) on Cu ions have been given. Spin-orbit coupling has not been considered in (a), and has been considered in (b).

(a)									
	FM			AFM-s			AFM-t		
energy	273.52			0.0			11.68		
gap	0.92			1.472			1.41		
Cu1-1	0	0	0.702	0	0	0.631	0	0	0.630
Cu1-2	0	0	0.702	0	0	0.631	0	0	0.630
Cu1-3	0	0	0.702	0	0	-0.631	0	0	-0.630
Cu1-4	0	0	0.702	0	0	-0.631	0	0	-0.630
Cu2-1	0	0	0.665	0	0	-0.648	0	0	-0.657
Cu2-2	0	0	0.665	0	0	0.648	0	0	0.657
Cu2-3	0	0	0.665	0	0	-0.648	0	0	-0.657
Cu2-4	0	0	0.665	0	0	0.648	0	0	0.657
Cu3-1	0	0	0.686	0	0	0.667	0	0	-0.674
Cu3-2	0	0	0.686	0	0	-0.667	0	0	0.674
Cu3-3	0	0	0.686	0	0	0.667	0	0	-0.674
Cu3-4	0	0	0.686	0	0	-0.667	0	0	0.674

(b)									
	FM			AFM-s			AFM-t		
energy	270.75			0.0			10.75		
gap	0.92			1.465			1.40		
Cu1-1	-0.002	0.054	0.697	0	0.013	0.629	0.002	0.037	0.627
Cu1-2	0.002	-0.054	0.697	0	0.013	0.629	-0.002	-0.037	0.627
Cu1-3	-0.002	-0.054	0.697	0	0.013	-0.629	-0.002	0.037	-0.627
Cu1-4	0.002	0.054	0.697	0	0.013	-0.629	0.002	-0.037	-0.627
Cu2-1	-0.008	0	0.663	0.014	-0.019	-0.642	0.015	0.004	-0.655
Cu2-2	0.008	0	0.663	0.014	-0.019	0.642	0.015	-0.004	0.655
Cu2-3	0.008	0	0.663	-0.014	-0.019	-0.642	-0.015	-0.004	-0.655
Cu2-4	-0.008	0	0.663	-0.014	-0.019	0.642	-0.015	0.004	0.655
Cu3-1	0.002	0	0.679	0.008	0.010	0.662	-0.008	0.012	-0.667
Cu3-2	-0.002	0	0.679	0.008	0.010	-0.662	-0.008	-0.012	0.667
Cu3-3	-0.002	0	0.679	-0.008	0.010	0.662	0.008	-0.013	-0.667
Cu3-4	0.002	0	0.679	-0.008	0.010	-0.662	0.008	0.013	0.667

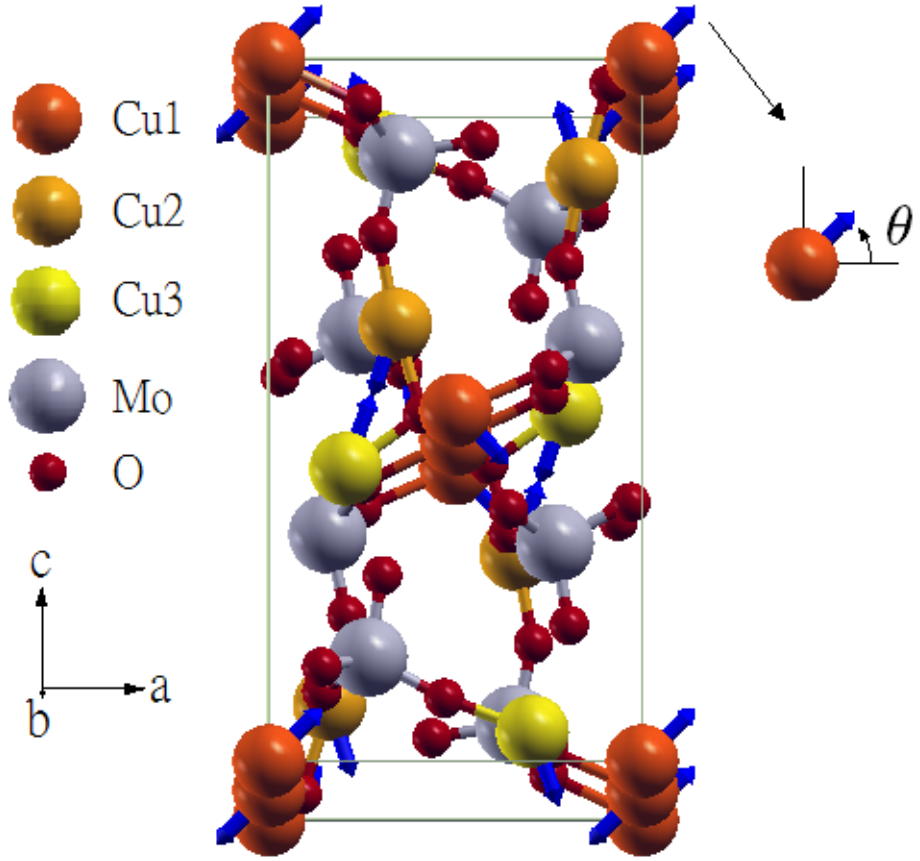

Figure 5.5: Calculated spin configurations are similar to the results of neutron diffraction experiments. All spins lie in the *ac*-plain almost. The spins on Cu1 form the AFM chain, and the spins on Cu2 and Cu3 form singlet dimers. We rotated the spins on Cu1 around the *b*-axis, while the spins on Cu2 and Cu3 remain fixed. The most stable noncollinear AFM spin configuration is that of an angle $\theta = 107^\circ$ or 287° between *a*-axis and direction of moments on Cu1.

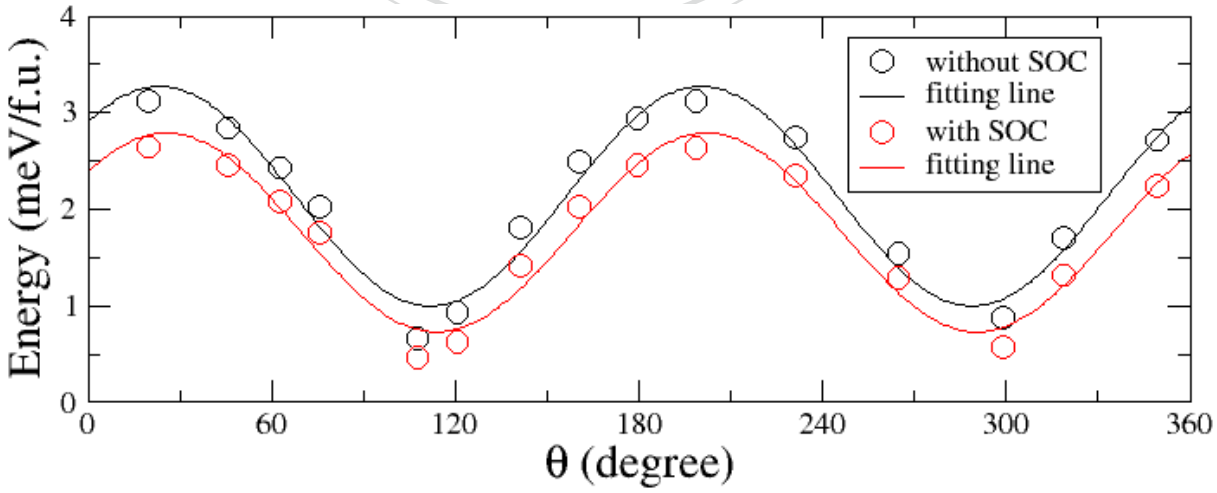

Figure 5.6: The energy versus θ of the spins on Cu1 in the system. The most stable noncollinear AFM spin configuration is that of an angle $\theta = 107^\circ$ or 287° approximately between *a*-axis and direction of the spins on Cu1.

Table 5.4: Non-collinear spin-polarized GGA+U calculations without the spin-orbit coupling. Energy (meV/unit cell), band gap (eV) and spin moments (μ_B) on Cu ions of spins configurations are given.

	θ=20°			θ=46°			θ=61°		
energy	12.50			11.37			9.72		
gap	1.46			1.46			1.47		
Cu1-1	0.596	0	0.212	0.442	0	0.452	0.292	0	0.560
Cu1-2	-0.596	0	0.212	-0.442	0	0.452	-0.292	0	0.560
Cu1-3	-0.596	0	-0.212	-0.442	0	-0.452	-0.292	0	-0.560
Cu1-4	0.596	0	-0.212	0.442	0	-0.452	0.292	0	-0.560
Cu2-1	-0.225	0	-0.606	-0.206	0	-0.613	-0.221	0	-0.608
Cu2-2	0.226	0	-0.606	0.206	0	-0.613	0.222	0	-0.607
Cu2-3	-0.226	0	0.606	-0.206	0	0.613	-0.222	0	0.607
Cu2-4	0.225	0	0.606	0.206	0	0.613	0.221	0	0.608
Cu3-1	0.236	0	0.624	0.211	0	0.633	0.230	0	0.627
Cu3-2	-0.234	0	0.625	-0.212	0	0.633	-0.228	0	0.627
Cu3-3	0.234	0	-0.625	0.212	0	-0.633	0.228	0	-0.627
Cu3-4	-0.236	0	-0.624	-0.212	0	-0.633	-0.230	0	-0.627

	θ=73°			θ=107°			θ=122°		
energy	8.09			2.68			3.75		
gap	1.47			1.47			1.47		
Cu1-1	0.188	0	0.603	-0.196	0	0.600	-0.323	0	0.542
Cu1-2	-0.188	0	0.603	0.196	0	0.600	0.323	0	0.542
Cu1-3	-0.188	0	-0.603	0.196	0	-0.600	0.323	0	-0.542
Cu1-4	0.188	0	-0.603	-0.196	0	-0.600	-0.323	0	-0.542
Cu2-1	-0.203	0	-0.614	-0.218	0	-0.609	-0.231	0	-0.604
Cu2-2	0.203	0	-0.614	0.217	0	-0.609	0.231	0	-0.604
Cu2-3	-0.203	0	0.614	-0.217	0	0.609	-0.231	0	0.604
Cu2-4	0.203	0	0.614	0.217	0	0.609	0.231	0	0.604
Cu3-1	0.208	0	0.634	0.239	0	0.623	0.241	0	0.622
Cu3-2	-0.208	0	0.634	-0.238	0	0.624	-0.240	0	0.623
Cu3-3	0.208	0	-0.634	0.237	0	-0.624	0.240	0	-0.623
Cu3-4	-0.208	0	-0.634	-0.239	0	-0.623	-0.241	0	-0.622

	θ=143°			θ=162°			θ=180°		
energy	7.26			9.95			11.78		
gap	1.46			1.46			1.46		
Cu1-1	-0.494	0	0.394	-0.596	0	0.211	-0.632	0	0.006
Cu1-2	0.494	0	0.394	0.596	0	0.211	0.632	0	0.006
Cu1-3	0.494	0	-0.394	0.596	0	-0.211	0.632	0	-0.006
Cu1-4	-0.494	0	-0.394	-0.596	0	-0.211	-0.632	0	-0.006
Cu2-1	-0.231	0	-0.604	-0.230	0	-0.604	-0.227	0	-0.605
Cu2-2	0.232	0	-0.603	0.231	0	-0.604	0.228	0	-0.605
Cu2-3	-0.232	0	0.603	-0.231	0	0.604	-0.228	0	0.605
Cu2-4	0.231	0	0.604	0.230	0	0.604	0.227	0	0.605
Cu3-1	0.243	0	0.622	0.242	0	0.622	0.238	0	0.623
Cu3-2	-0.241	0	0.622	-0.240	0	0.623	-0.237	0	0.624
Cu3-3	0.241	0	-0.622	0.240	0	-0.623	0.237	0	-0.624
Cu3-4	-0.243	0	-0.622	-0.242	0	-0.622	-0.239	0	-0.623

	θ=200°			θ=230°			θ=265°		
energy	12.50			10.98			6.17		
gap	1.46			1.47			1.48		
Cu1-1	-0.600	0	-0.199	-0.397	0	-0.491	-0.059	0	-0.629
Cu1-2	0.600	0	-0.199	0.397	0	-0.491	0.003	0	-0.631
Cu1-3	0.600	0	0.199	0.397	0	0.491	0.059	0	0.629
Cu1-4	-0.600	0	0.199	-0.397	0	0.491	-0.003	0	0.631
Cu2-1	-0.226	0	-0.606	-0.222	0	-0.607	-0.237	0	-0.601
Cu2-2	0.226	0	-0.606	0.223	0	-0.607	0.239	0	-0.601
Cu2-3	-0.226	0	0.606	-0.223	0	0.607	-0.239	0	0.601
Cu2-4	0.225	0	0.606	0.222	0	0.607	0.237	0	0.601
Cu3-1	0.236	0	0.624	0.232	0	0.626	0.220	0	0.630
Cu3-2	-0.234	0	0.625	-0.230	0	0.627	-0.217	0	0.631
Cu3-3	0.234	0	-0.625	0.230	0	-0.627	0.217	0	-0.631
Cu3-4	-0.236	0	-0.624	-0.232	0	-0.626	-0.220	0	-0.630

	θ=290°			θ=320°			θ=350°		
energy	3.49			6.84			10.88		
gap	1.47			1.46			1.46		
Cu1-1	0.308	0	-0.551	0.475	0	-0.416	0.621	0	-0.120
Cu1-2	-0.308	0	-0.551	-0.475	0	-0.416	-0.621	0	-0.120
Cu1-3	-0.308	0	0.551	-0.475	0	0.416	-0.621	0	0.120
Cu1-4	0.308	0	0.551	0.475	0	0.416	0.621	0	0.120
Cu2-1	-0.231	0	-0.604	-0.231	0	-0.604	-0.229	0	-0.605
Cu2-2	0.231	0	-0.604	0.232	0	-0.603	0.230	0	-0.604
Cu2-3	-0.231	0	0.604	-0.232	0	0.603	-0.230	0	0.604
Cu2-4	0.230	0	0.604	0.231	0	0.604	0.229	0	0.605
Cu3-1	0.241	0	0.622	0.243	0	0.622	0.240	0	0.623
Cu3-2	-0.239	0	0.623	-0.241	0	0.622	-0.239	0	0.623
Cu3-3	0.239	0	-0.623	0.241	0	-0.622	0.239	0	-0.624
Cu3-4	-0.241	0	-0.622	-0.243	0	-0.622	-0.241	0	-0.623

Table 5.5: Non-collinear spin-polarized GGA+U calculations with the spin-orbit coupling. Energy (meV/unit cell), band gap (eV) and spin moments (μ_B) on Cu ions of spins configurations we found have been given.

	θ=20°			θ=46°			θ=61°		
energy	10.58			9.84			8.31		
gap	1.44			1.45			1.46		
Cu1-1	0.591	0.043	0.212	0.437	0.038	0.451	0.290	0.031	0.558
Cu1-2	-0.591	0.043	0.212	-0.437	0.039	0.451	-0.290	0.031	0.558
Cu1-3	-0.591	0.043	-0.212	-0.437	0.039	-0.451	-0.290	0.031	-0.558
Cu1-4	0.591	0.043	-0.212	0.437	0.038	-0.451	0.290	0.031	-0.558
Cu2-1	-0.213	-0.010	-0.606	-0.195	-0.014	-0.611	-0.209	-0.016	-0.607
Cu2-2	0.213	-0.009	-0.606	0.195	-0.014	-0.611	0.210	-0.016	-0.607
Cu2-3	-0.213	-0.009	0.606	-0.195	-0.014	0.612	-0.210	-0.016	0.607
Cu2-4	0.213	-0.009	0.606	0.195	-0.014	0.612	0.209	-0.016	0.607
Cu3-1	0.245	-0.008	0.614	0.220	-0.002	0.624	0.240	0.003	0.616
Cu3-2	-0.244	-0.008	0.615	-0.220	-0.002	0.624	-0.238	0.003	0.617
Cu3-3	0.243	-0.008	-0.615	0.220	-0.002	-0.624	0.238	0.003	-0.617
Cu3-4	-0.245	-0.008	-0.614	-0.220	-0.002	-0.624	-0.240	0.003	-0.616

	θ=73°			θ=107°			θ=122°		
energy	7.02			1.87			2.51		
gap	1.46			1.47			1.46		
Cu1-1	0.189	0.025	0.600	-0.191	0.001	0.599	-0.320	-0.008	0.541
Cu1-2	-0.189	0.025	0.600	0.191	0.002	0.599	0.320	-0.008	0.541
Cu1-3	-0.189	0.025	-0.600	0.191	0.002	-0.599	0.320	-0.008	-0.541
Cu1-4	0.189	0.025	-0.600	-0.191	0.001	-0.599	-0.320	-0.008	-0.541
Cu2-1	-0.193	-0.016	-0.612	-0.212	-0.017	-0.606	-0.217	-0.012	-0.604
Cu2-2	0.193	-0.016	-0.612	0.212	-0.017	-0.606	0.218	-0.012	-0.604
Cu2-3	-0.193	-0.016	0.612	-0.212	-0.017	0.606	-0.218	-0.012	0.604
Cu2-4	0.193	-0.016	0.612	0.212	-0.017	0.606	0.217	-0.012	0.604
Cu3-1	0.217	0.005	0.625	0.242	0.015	0.616	0.249	0.017	0.613
Cu3-2	-0.217	0.005	0.625	-0.240	0.015	0.616	-0.247	0.017	0.613
Cu3-3	0.217	0.005	-0.625	0.240	0.015	-0.616	0.247	0.017	-0.613
Cu3-4	-0.217	0.005	-0.625	-0.242	0.015	-0.616	-0.249	0.017	-0.613

	θ=143°			θ=162°			θ=180°		
energy	5.65			8.11			9.81		
gap	1.46			1.44			1.44		
Cu1-1	-0.490	-0.022	0.393	-0.592	-0.033	0.210	-0.628	-0.041	0.006
Cu1-2	0.490	-0.022	0.393	0.592	-0.033	0.210	0.628	-0.041	0.006
Cu1-3	0.490	-0.022	-0.393	0.592	-0.033	-0.210	0.628	-0.040	-0.005
Cu1-4	-0.490	-0.022	-0.393	-0.592	-0.033	-0.210	-0.628	-0.041	-0.006
Cu2-1	-0.218	-0.006	-0.604	-0.216	-0.001	-0.605	-0.215	0.004	-0.605
Cu2-2	0.219	-0.006	-0.604	0.217	-0.001	-0.604	0.215	0.005	-0.605
Cu2-3	-0.218	-0.006	0.604	-0.217	0	0.604	-0.215	0.005	0.605
Cu2-4	0.218	-0.006	0.604	0.216	0	0.605	0.215	0.005	0.605
Cu3-1	0.250	0.016	0.612	0.249	0.014	0.612	0.248	0.012	0.613
Cu3-2	-0.248	0.016	0.613	-0.247	0.014	0.613	-0.246	0.012	0.614
Cu3-3	0.248	0.016	-0.613	0.247	0.014	-0.613	0.246	0.012	-0.614
Cu3-4	-0.250	0.016	-0.612	-0.249	0.014	-0.612	-0.248	0.012	-0.613

	θ=200°			θ=230°			θ=265°		
energy	10.57			9.41			5.15		
gap	1.44			1.45			1.47		
Cu1-1	-0.595	-0.043	-0.200	-0.394	-0.037	-0.490	-0.058	-0.020	-0.626
Cu1-2	0.595	-0.043	-0.200	0.394	-0.037	-0.490	0.002	-0.016	-0.629
Cu1-3	0.595	-0.043	0.200	0.394	-0.037	0.490	0.058	-0.019	0.626
Cu1-4	-0.595	-0.043	0.200	-0.394	-0.037	0.490	-0.002	-0.015	0.629
Cu2-1	-0.213	0.009	-0.606	-0.210	0.015	-0.607	-0.222	0.020	-0.602
Cu2-2	0.214	0.009	-0.606	0.210	0.015	-0.606	0.223	0.021	-0.602
Cu2-3	-0.213	0.009	0.606	-0.210	0.015	0.606	-0.223	0.021	0.602
Cu2-4	0.213	0.009	0.606	0.210	0.015	0.607	0.222	0.020	0.602
Cu3-1	0.246	0.008	0.614	0.242	0	0.616	0.233	-0.011	0.619
Cu3-2	-0.244	0.008	0.615	-0.240	0	0.617	-0.231	-0.009	0.620
Cu3-3	0.244	0.008	-0.615	0.240	0	-0.617	0.231	-0.009	-0.620
Cu3-4	-0.246	0.008	-0.614	-0.242	0	-0.616	-0.233	-0.011	-0.619

	θ=290°			θ=320°			θ=350°		
energy	2.32			5.28			8.98		
gap	1.46			1.46			1.44		
Cu1-1	0.306	0.007	-0.549	0.472	0.020	-0.415	0.617	0.037	-0.119
Cu1-2	-0.306	0.007	-0.549	-0.472	0.020	-0.415	-0.617	0.037	-0.119
Cu1-3	-0.306	0.007	0.549	-0.472	0.021	0.415	-0.617	0.037	0.119
Cu1-4	0.306	0.007	0.549	0.472	0.020	0.415	0.617	0.037	0.119
Cu2-1	-0.217	0.013	-0.604	-0.218	0.006	-0.604	-0.216	-0.002	-0.605
Cu2-2	0.218	0.013	-0.604	0.219	0.006	-0.604	0.217	-0.002	-0.605
Cu2-3	-0.218	0.013	0.604	-0.219	0.006	0.604	-0.216	-0.002	0.605
Cu2-4	0.217	0.013	0.604	0.218	0.006	0.604	0.216	-0.002	0.605
Cu3-1	0.248	-0.017	0.613	0.250	-0.016	0.612	0.249	-0.013	0.613
Cu3-2	-0.247	-0.017	0.614	-0.248	-0.016	0.613	-0.247	-0.013	0.613
Cu3-3	0.247	-0.017	-0.614	0.248	-0.016	-0.613	0.247	-0.013	-0.614
Cu3-4	-0.248	-0.017	-0.613	-0.250	-0.016	-0.612	-0.249	-0.013	-0.613

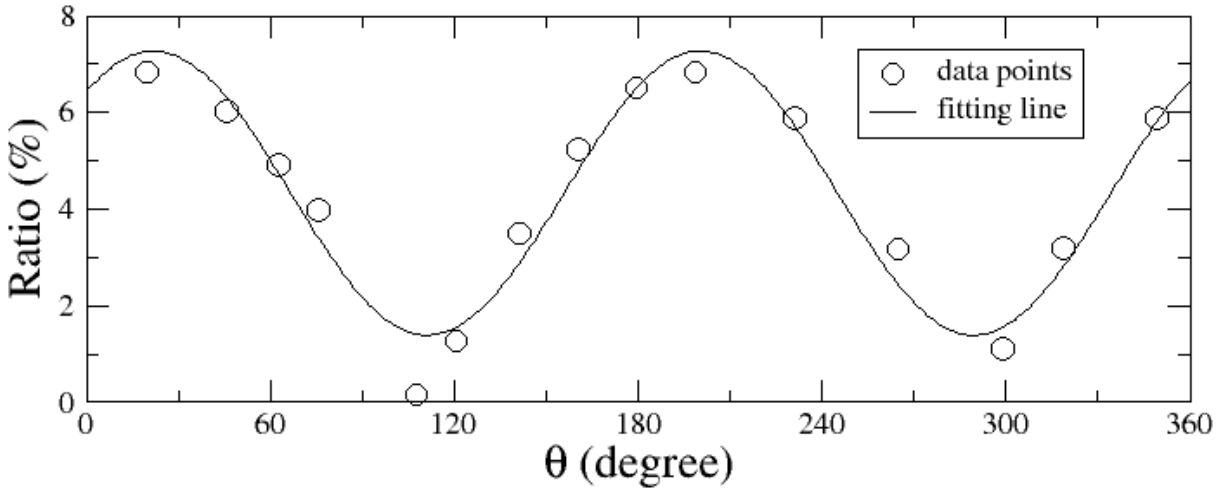

Figure 5.7: All spins lie in the *ac*-plane in the most stable noncollinear AFM spin configuration, i.e. an angle $\theta = 107^\circ$ or 287° between *a*-axis and direction of spins of Cu1. When the spins on Cu1 rotate to another angle, the spins cant away from the *ac*-plane occur, especially on Cu1.

parameter here means that the two corresponding spins tend to point along the oppsite directions. For simplicity, here we only consider the nearest interaction between Cu_i and Cu_j atoms, and the second-nearest interaction between Cu1 atoms. The four exchange parameters (J_1, J_2, J_3 and J_4) correspond to nearest Cu-Cu interactions (Cu_1-Cu_2, Cu_1-Cu_3, Cu_2-Cu_3 and Cu_1-Cu_1) in the system. And the second-nearest interaction between Cu1 atoms is labeled as J_5. To obtain these five parameters, we performed a series of collinear spin-polarized calculations. The results are listed in Table 5.6. Through solving the equations,

$$H = H_0 + H_{mag} + H_{eff}, \tag{5.2}$$

where H_0 is the internal energy of the system, H_{mag} is the magnetization energy and H_{eff} is the Hamiltonian of the effective Heisenberg model. we can obtain the exchange parameters.

$$\begin{aligned}
E_{singlet} &= E_0 + 8J_3 + 8J_4 - 4J_5 = 0 \\
E_{triplet} &= E_0 - 8J_3 + 8J_4 - 4J_5 = 23.36 \\
E_{(a)} &= E_0 - 8J_1 - 8J_2 - 8J_3 - 4J_5 = 306.92 \\
E_{(b)} &= E_0 - 8J_1 - 16J_2 - 4J_3 - 8J_4 - 4J_5 = 531.02 \\
E_{(c)} &= E_0 - 8J_1 - 8J_2 - 8J_3 - 8J_4 - 4J_5 = 521.60 \\
E_{(d)} &= E_0 - 8J_1 - 8J_2 - 8J_3 - 4J_4 = 424.24 \quad .
\end{aligned} \tag{5.3}$$

The results are listed in Table 5.7. The two of parameters (J_1 and J_5) are positive, and the remaining are negative. It is impossible to simultaneously minimize the energy of all exchange interactions. As is mentioned before, geometric frustration possibly plays an important role in this system. The two strongest exchange interaction, J_4 and J_5, would lead to the Cu1 AFM

Table 5.6: A series of collinear spin-polarized GGA+U calculations. To obtain the four parameters (J_1, J_2, J_3 and J_4), we performed a series of collinear spin-polarized calculations concluding ferromagnetic configuration and some ferrimagnetic configurations which randomly flip spins in the unit cell. Energy (meV/2 unit cell) and spin moments (μ_B) on Cu ions are listed.

	AFM-s	AFM-t	(a)	(b)	(c)	(d)	
energy	0	23.36	306.92	531.02	521.60	424.24	
Cu1-1(5)	0.631	0.630	0.701	0.692	0.687	−0.643	0.669
Cu1-2(6)	0.631	0.630	0.642	0.702	0.702	0.701	0.701
Cu1-3(7)	−0.631	−0.630	0.701	0.692	0.687	−0.642	0.669
Cu1-4(8)	−0.631	−0.630	−0.618	0.701	0.701	0.701	0.701
Cu2-1(5)	−0.648	−0.657	0.659	0.664	0.664	0.659	0.659
Cu2-2(6)	0.648	0.657	0.665	0.664	0.664	0.665	0.665
Cu2-3(7)	−0.648	−0.657	0.665	−0.643	−0.654	0.665	0.665
Cu2-4(8)	0.648	0.657	0.659	0.665	0.664	0.657	0.663
Cu3-1(5)	0.667	−0.674	0.679	0.685	0.684	0.685	0.686
Cu3-2(6)	−0.667	0.674	0.685	0.685	0.681	0.679	0.679
Cu3-3(7)	0.667	−0.674	0.685	0.675	−0.668	0.677	0.684
Cu3-4(8)	−0.667	0.674	0.679	0.685	0.685	0.685	0.685

Table 5.7: The distance D between Cu ions is listed and the exchange parameters (meV) in (a) our results qualitatively agree with (b) the experimental results (only J_3 and J_4 obtained in the experiments).

	J_1 (Cu1-Cu2)	J_2 (Cu1-Cu3)	J_3 (Cu2-Cu3)	J_4 (Cu1-Cu1)	J_5 (Cu1-Cu1)
D	2.97Å	2.98Å	3.17Å	3.44Å	6.88Å
(a)	0.4375	-1.9075	-1.460	-26.835	2.50
(b)			-4.0	-22.0	

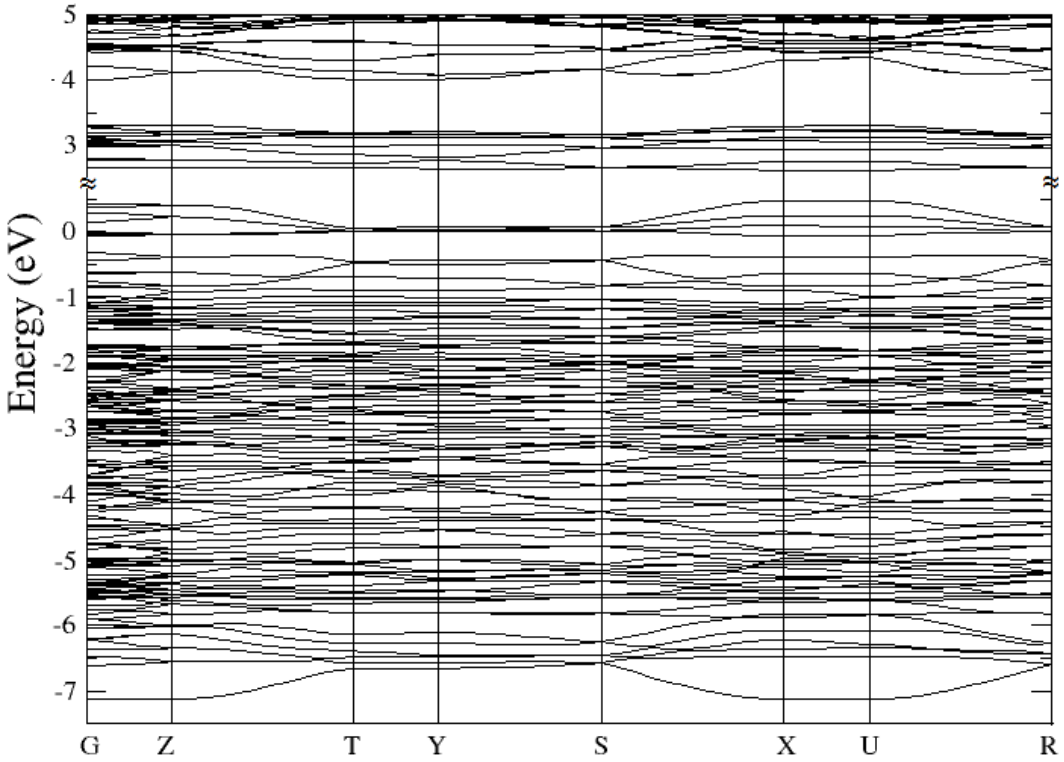

Figure 5.8: The NM electronic band structure.

chain. The exchange parameter J_3 which is larger than J_1 and J_2 would lead to singlet dimer formed by Cu2 and Cu3. The singlet dimers weakly interact with the Cu_1 chain. Our results agree with the experimental results well (only J_3 and J_4 obtained in the experiments). The strength of J_4 we obtained is slightly larger than result of experiments. And J_3 is slightly smaller. When considering the relativistic effect, the spins cant away from the ac-plane, especially on Cu1, as can be seen in Table 5.5. We think that the exchange interactions tend to make spins lie in the *ac*-plane, and the relativistic effect tends to make spins cant along the *b*-axis. When spins on Cu1 rotate away from the more stable pointings ($\theta = 107^\circ$ or 287° between *a*-axis and direction of the spins on Cu1), the dominance of exchange interactions decrease and *b*-component of spins increase. Therefore, the spins on Cu1 cant the most in the FM state.

5.5 Electronic Structure

We ploted the electronic band structure and densities of states of our NM calculations in Figure 5.8 and 5.9. The lowest valence band at the Γ point is dominant Cu1-d_{xy} hybridized with O1-p_y orbitals in the vicinity of -7.1 eV with bandwidth of about 0.5 eV. In the vicinity of -5.75 eV and -5.5 eV, bands are dominated by the Cu2-d_{z^2} orbital hybridized with O6-p_z orbital and Cu3-$d_{x^2-y^2}$ orbital hybridized with O5-p_x orbital. Above -5.5 eV and below -0.5 eV, bands are too complex to be recognized. In the vicinity of -0.4 eV, bands are dominated by the Cu3-$d_{x^2-y^2}$ and the Cu3-d_{zx} orbitals hybridized with O1-p_x orbital. The NM state is

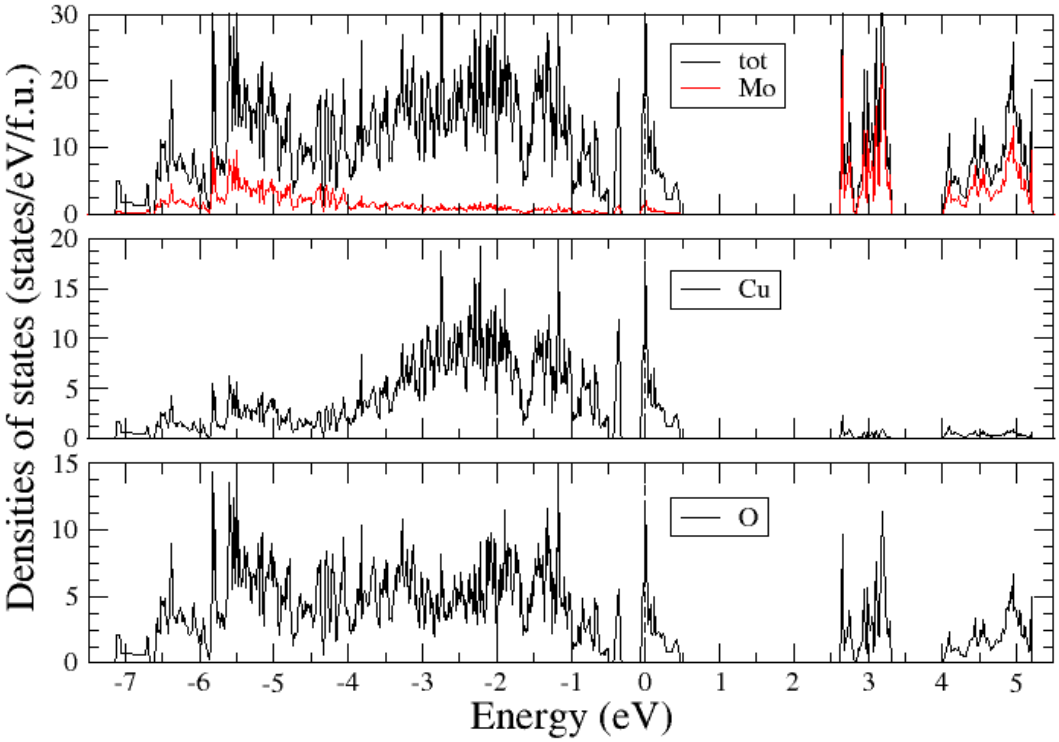

Figure 5.9: Total and site-projected electronic densities of states of the NM state.

metallic, and the bands crossing the Fermi level are dominated by Cu2-d_{z^2} orbital hybridized with O1-p_z and O2-p_y orbitals, and by Cu3-$d_{x^2-y^2}$ and Cu3-d_{zx} orbitals hybridized with O1-p_x, O1-p_z and O3-p_y orbitals. In the vicinity of 0.4 eV, bands are dominated by Cu1-$d_{x^2-y^2}$ and Cu1-d_{xy} orbitals hybridized with O1-p_y orbital. Above 2.5 eV, bands are dominated by orbitals of Mo atoms hybridized with p-orbitals of the surrounding O atoms.

Here we look into orbital- and site-projected DOS of Cu atoms more closely to examine the crystal field theory. The Cu1 ion and its surrounding O ions (two O1 and two O3 ions) form a parallelogram, and the nearest ligands are O1 ions (1.86 $\AA$) which must affect the splitting of d-orbitals of Cu1 the most, while O2 (2.30 $\AA$) ions are too far away from the Cu1 ion to cause considerable splitting. There is an angle of about 21° between y-axis and the direction that O1 ion attached to the central Cu1 ion along, and an angle of about 25° between x-axis and the direction that O3 ion attached to the central Cu1 ion along. We infered that $d_{x^2-y^2}$ and d_{xy} orbitals must correspond to the high energy levels. Since O3 ions have longer bond length, d_{z^2} and d_{zx} orbitals must correspond to low energy levels. And the d_{yz} orbital must correspond to the lowest energy level. As can be seen in Figure 5.10 of Cu1, in the vicinity of about 0.4 eV, $d_{x^2-y^2}$ and d_{xy} orbitals have almost same DOS, due to locations of O1 ions that $d_{x^2-y^2}$ and d_{xy} orbitals experience almost same strength Coulomb repulsion. In the vicinity of about -0.6 eV, d_{z^2} and d_{zx} orbitals dominate and must correspond to higher energy level than d_{yz} orbital. In the same way, the Cu2 ion and its surrounding O ions (one O1, two O2 and one O6 ions) form a quadrangle-like structure, the nearest ligands are O6 ions which must lead to the largest effect of splitting of the d-orbitals, while O7 ions are too far away from the Cu2 ion to cause

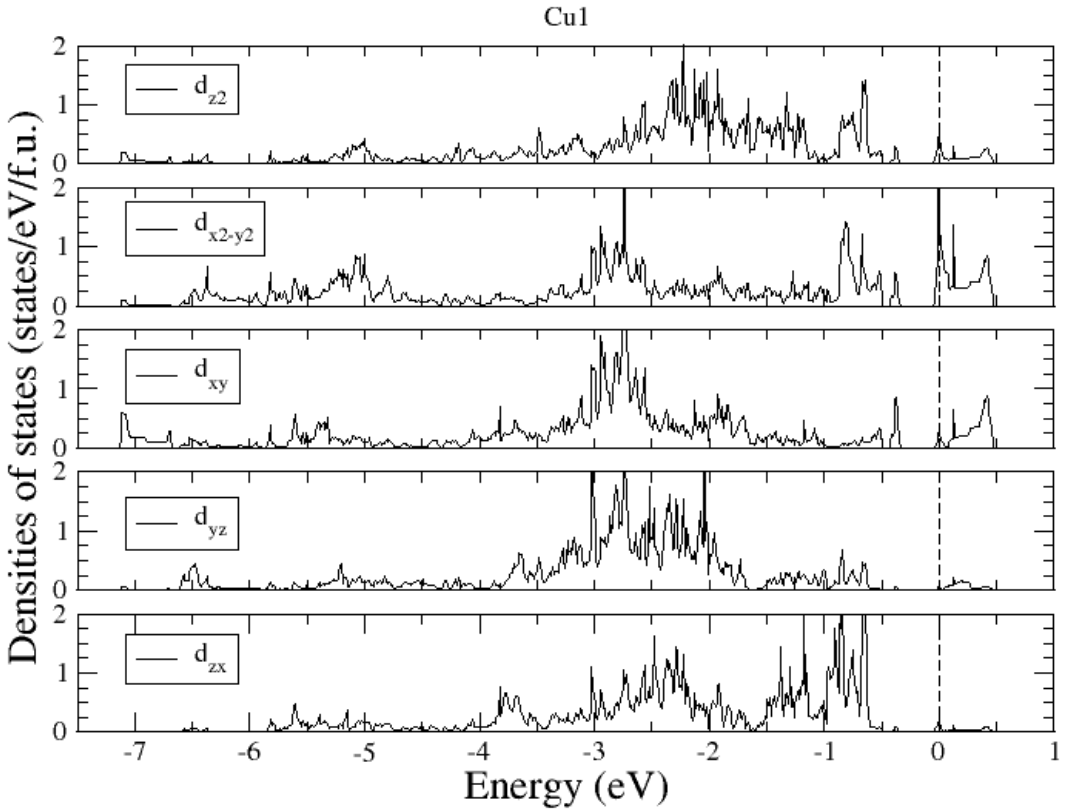

Figure 5.10: NM orbital- and site-projected electronic densities of states of Cu1 atoms.

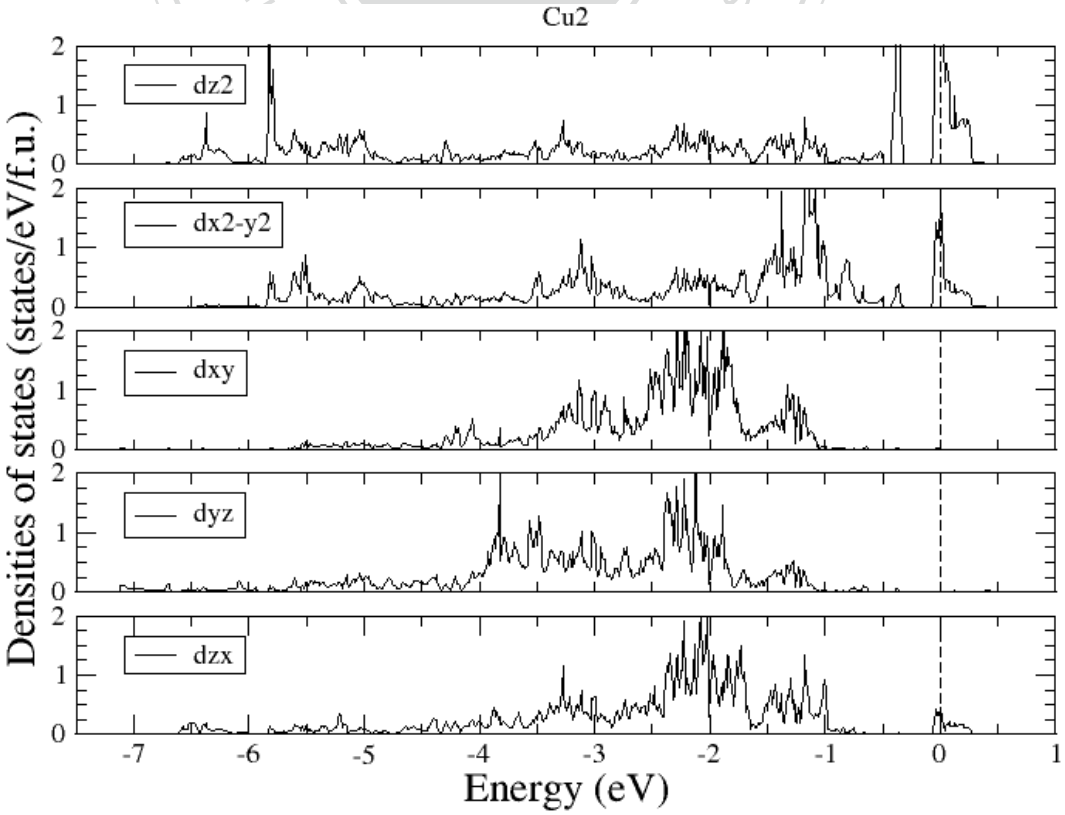

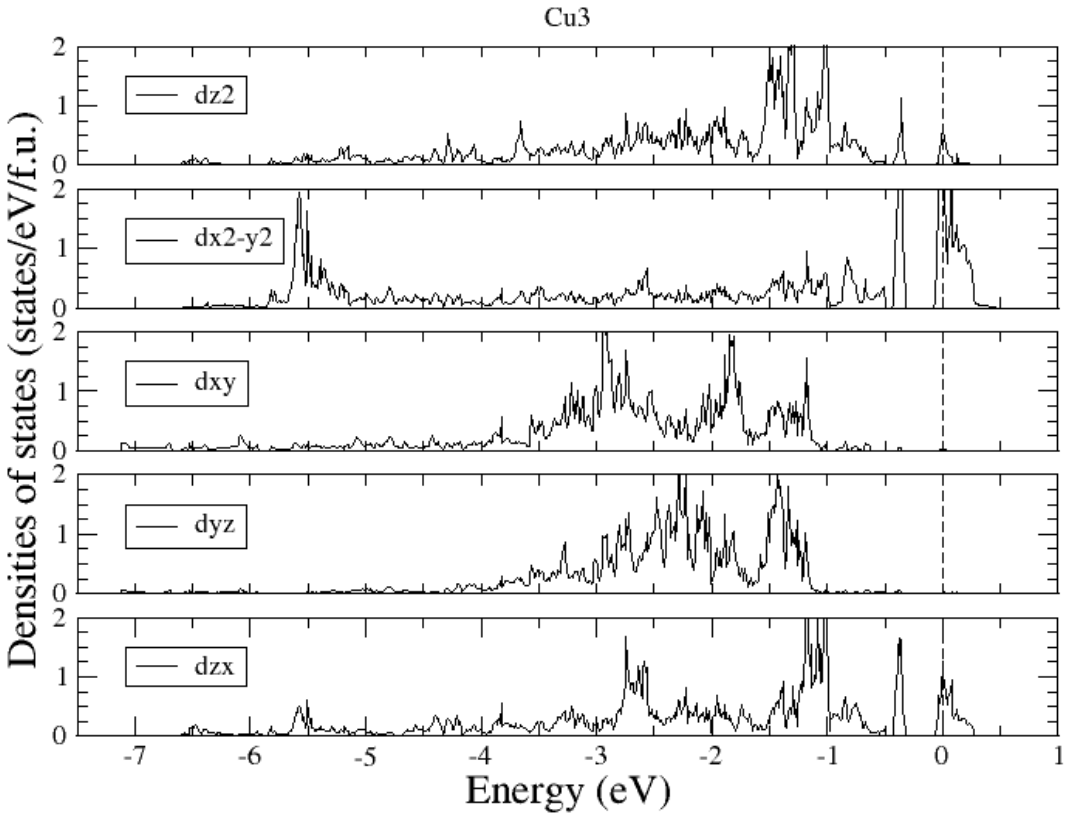

Figure 5.11: NM orbital- and site-projected electronic densities of states of Cu2 and Cu3 atoms.

the considerable effect. The quadrangle-like structure almost lie in yz-plane. Since O1, O2 and O6 ions almost attached to the central Cu2 ion along the y and z axes, d_{z^2} and $d_{x^2-y^2}$ orbitals must correspond to higher energy levels than remaining d_{xy}, d_{yz} and d_{zx} orbitals. As can be seen in Figure 5.11 of Cu2, the results agree with our expectation generally. The Cu3 and its surrounding O ions (one O1, two O3 and one O5 ions) also form a quadrangle-like structure, The nearest ligands are O5 ions which can lead to the largest effect of splitting of the d-orbitals, while the surrounding O4 and O7 ions are too far away from the Cu3 ion to cause considerable effects. The two O3 and one O5 ions attached to the central Cu3 ion along y-axis and x-axis almost. Therefore, the $d_{x^2-y^2}$ orbital must correspond to high energy levels. The O1 ion lie in-between the x and z axes, pushing that d_{zx} orbital also to higher energy level. The remaining orbitals experience smaller electron-electron Coulomb repulsion so that they stay in the lower energy levels. As can be seen in Figure 5.11 of Cu3, the results agree with our expectation. By the way, those bands across the Fermi level signify that ions near corresponding d-orbitals experience less Coulomb repulsion, causing shorter bond length. Our results agree with crystal field theory well.

Then, we ploted the electronic band structure and densities of states of the collinear FM state from our collinear spin-polarized GGA+U calculations in Figure 5.12 and 5.13. As mentioned before, the lowest valence band at the Γ point is the dominant Cu1-d_{xy} band hybridized with O1-p_y orbital near -7.1 eV in the NM state. When considering the spin-polarization, in the collinear

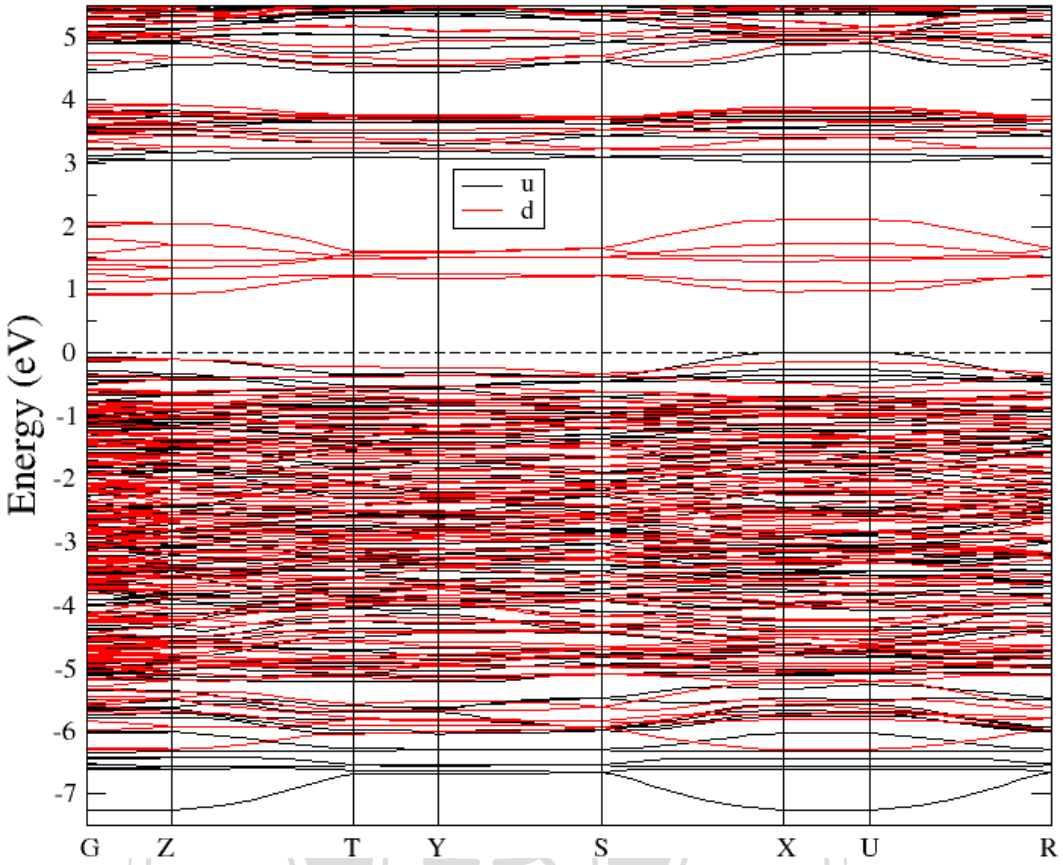

Figure 5.12: The electronic band structure of the collinear FM state from the collinear spin-polarized GGA+U calculations.

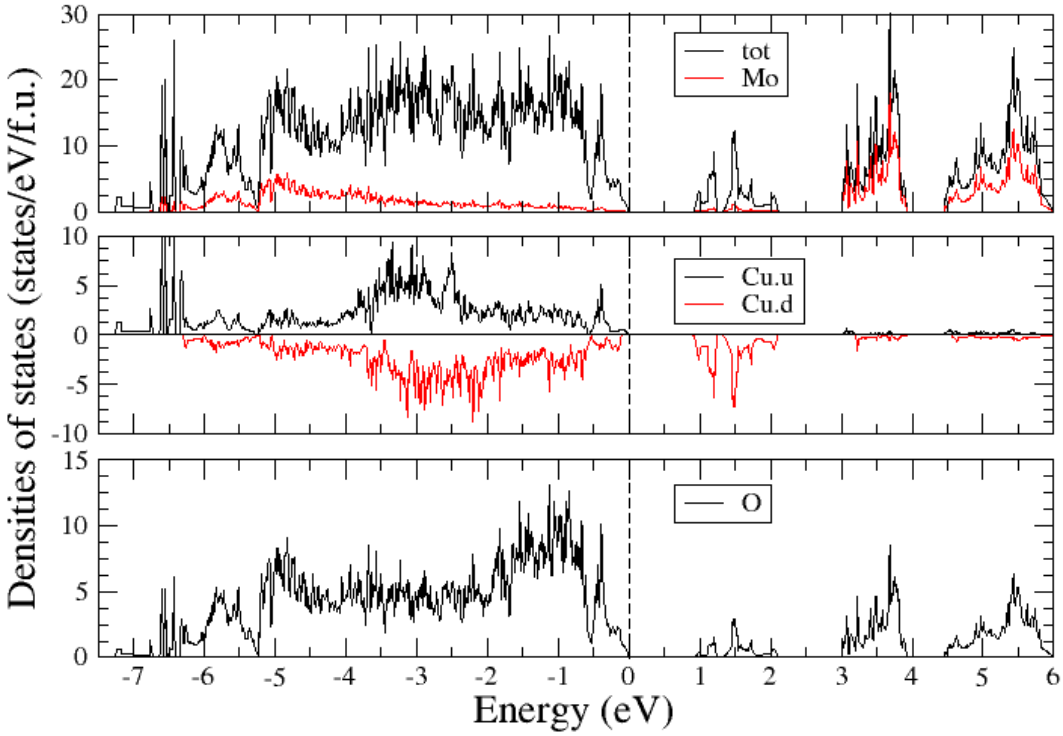

Figure 5.13: Total and site-projected electronic densities of states of the collinear FM state from the collinear spin-polarized GGA+U calculations.

FM state which is listed in Table 5.3 (b), the band split into two bands (spin up and down) between -7.26 eV and -6.3 eV. Besides, considerable states dominated by Cu1-$d_{x^2-y^2}$ orbital hybridized with O1-p_y orbital appear in the lowest valence band at about -7.26 eV. Near -6.6 eV, spin-up bands are Cu2-d_{z^2} orbital hybridized with O1-p_z and O6-p_z orbitals. Here it should be mentioned that bands are dominated by Cu2-d_{z^2} orbital hybridized with mainly O6-p_z orbital in the vicinity of about -5.75 eV in the NM state. There must be some transferring of electrons after considering spin-polarization. At about -6.4 eV, spin-up bands are Cu3-$d_{x^2-y^2}$ orbital hybridized with O5-p_x orbital and Cu3-d_{zx} orbital hybridized with O1-p_x orbital. Likewise, there must be some transferring of electrons infered from the appearance of the band dominated by corresponding Cu3-d_{zx} orbital hybridized with O1-p_x orbital after considering spin-polarization. The highest occupied spin-up and spin-down bands are dominated by corresponding Cu1-$d_{x^2-y^2}$ and Cu1-d_{xy} orbitals hybridized with O1-p_y orbital. An energy gap (0.92 eV) has been opened here. Those spin-down bands in the interval between about 1.0 eV and 2.0 eV are effects of considering Coulomb repulsion of electrons. A spin-down electron can occupy those orbitals only if it overcomes the Hubbard U. In the energy range between 1.0 eV and 2.0 eV, bands are the dominantly Cu1-$d_{x^2-y^2}$ and Cu1-d_{xy} orbitals. In the vicinity of 1.2 eV, bands are mainly Cu3-$d_{x^2-y^2}$ and Cu3-d_{zx} orbitals. And near 1.5 eV, bands are dominant Cu2-d_{z^2} orbital slightly hybridized with O1-p_z orbital. Above 3.0 eV, bands are dominated by orbitals of Mo atoms hybridized with p-orbitals of the surrounding O atoms.

We also ploted the electronic band structure and densities of states of the collinear AFM-t and AFM-s states (Table 5.3 (b)) in Figure 5.14, 5.15, 5.16 and 5.17. The electronic structure of the two states are similar, the main difference between them that we can recognize are located in the vicinity of 1.5 eV. The lowest valence band is also the dominant Cu1-d_{xy} band hybridized with O1-p_y orbital at -6.6 eV. However, the bandwidth is narrowed to about 0.2 eV. The bands dominated by Cu2-d_{z^2} orbital hybridized with O1-p_z and O6-p_z orbitals in the collinear FM state rise to about -6.4 eV in the collinear AFM state. And, the bands dominated by Cu3-$d_{x^2-y^2}$ orbital hybridized with O5-p_x orbital and Cu3-d_{zx} orbital hybridized with O1-p_x orbital rise to about -6.05 eV. Likewise, bands above -6 eV and below -0.5 eV are too complex to be recognized. The highest occupied band with narrow bandwidth of about 0.1 eV is dominated by Cu1-d_{zx} orbital hybridized with O2-p_z and O3-p_x orbitals, and Cu1-d_{z^2} orbital hybridized with O2-p_z orbital. A reasonable energy gap of 1.41 eV was obtained in the AFM-t state, and increases to 1.472 eV in the AFM-s state. In the intervals between 1.35 eV and 1.8 eV, there is a series of narrow conduction bands. In the AFM-t state, the lowest unoccupied bands in the vicinity of 1.35 eV are dominated by Cu3-$d_{x^2-y^2}$ and Cu3-d_{zx} orbitals. The bands pushed up to about 1.5 eV in the AFM-s state. Near 1.63 eV is mainly Cu2-d_{z^2} orbital slightly hybridized with O1-p_z orbital in the AFM-t state, and it rises slightly in the AFM-s state. The highest bands of the series of the bands in the vicinity of 1.75 eV is dominated by Cu1-$d_{x^2-y^2}$ and Cu1-d_{xy} orbitals in the AFM-t state. The bands do not move apparently in the AFM-s state. Above 3 eV, bands are dominated by orbitals of Mo atoms hybridized with p-orbitals of the surrounding O

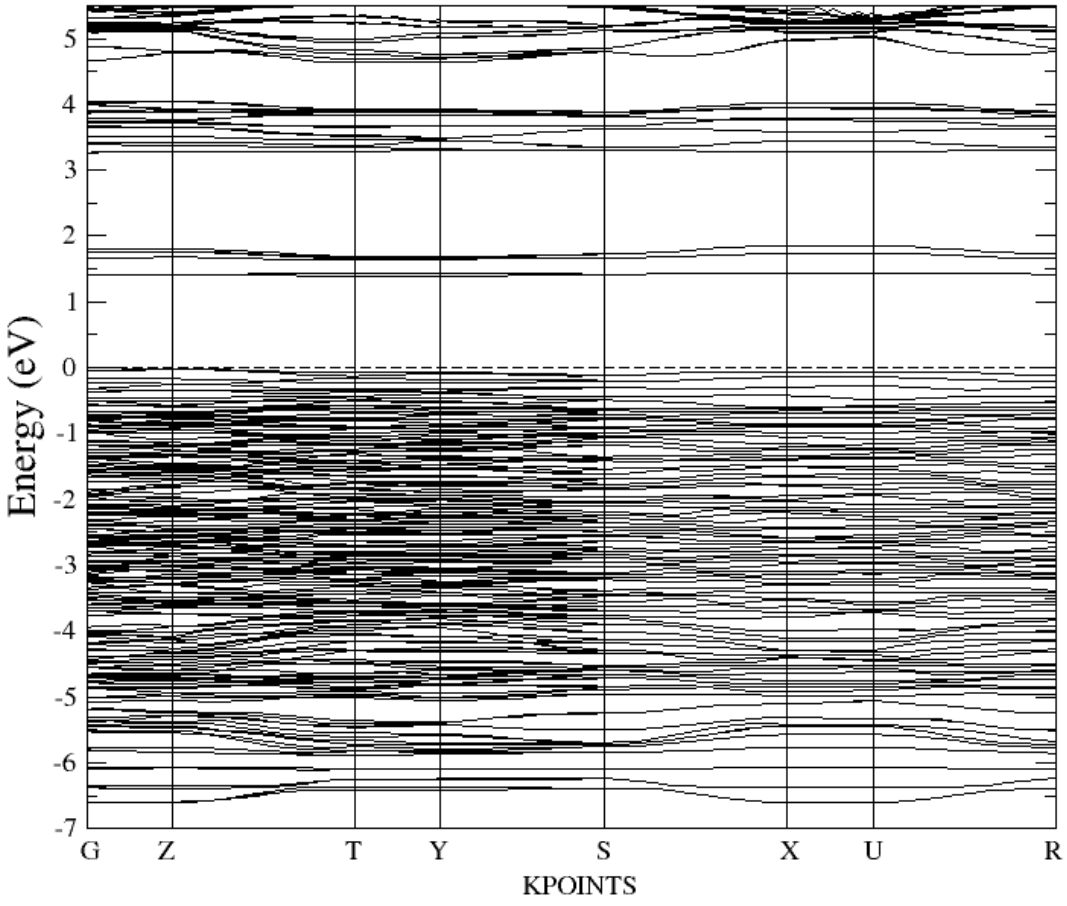

Figure 5.14: The electronic band structure of the collinear AFM-t state from the collinear spin-polarized GGA+U calculations.

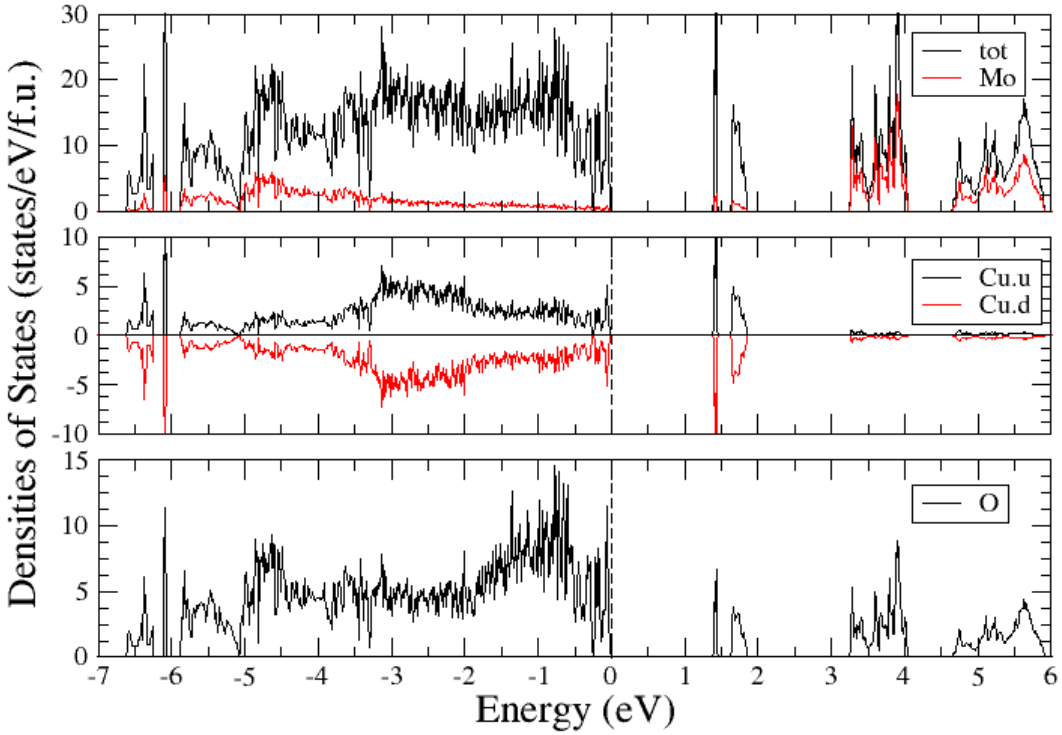

Figure 5.15: Total and site-projected electronic densities of states of the collinear AFM-t state from the collinear spin-polarized GGA+U calculations.

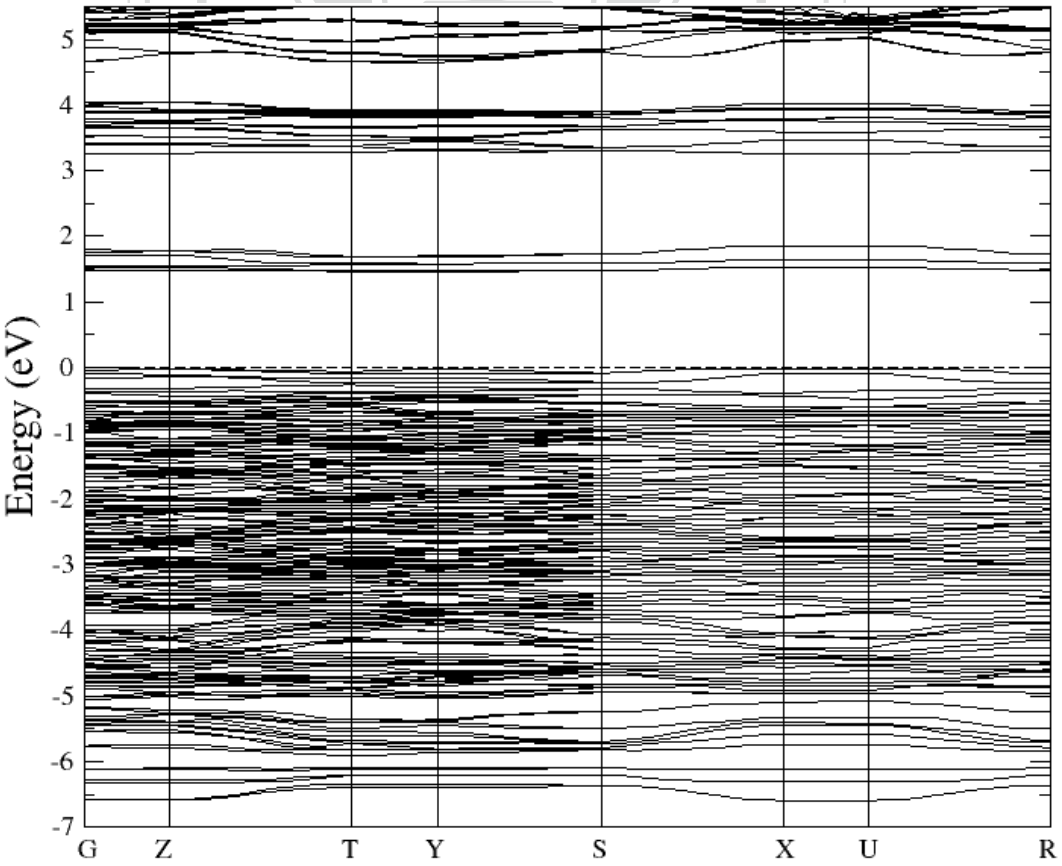

Figure 5.16: The electronic band structure of the collinear AFM-s state from the collinear spin-polarized GGA+U calculations.

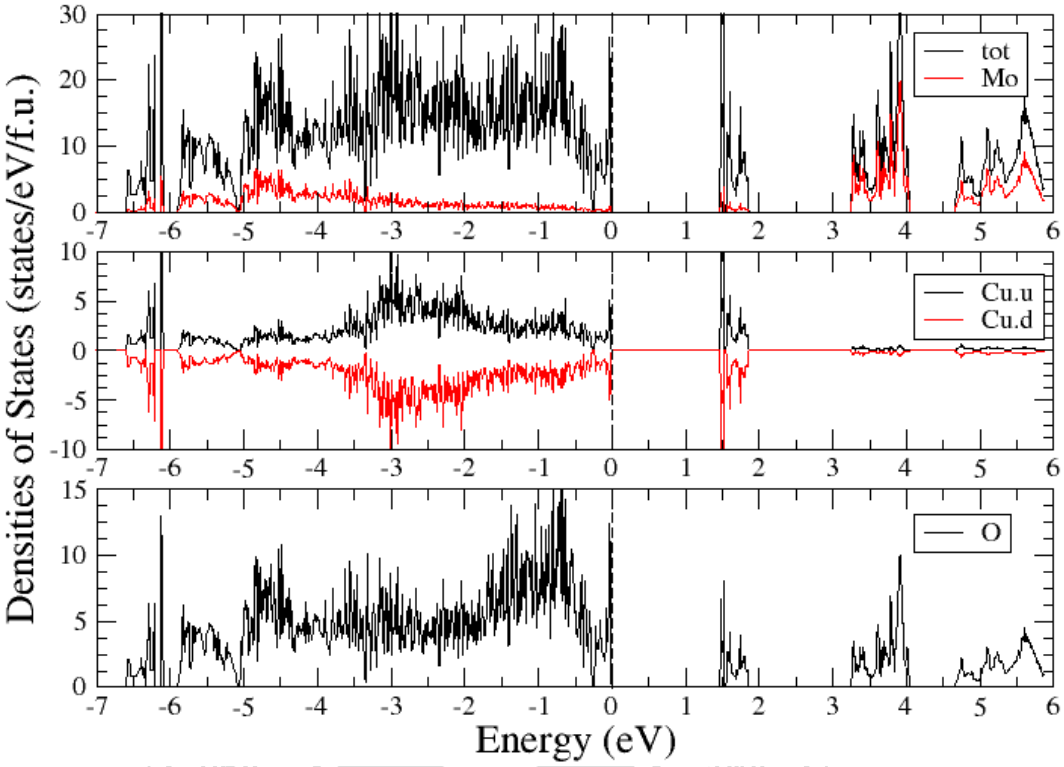

Figure 5.17: Total and site-projected electronic densities of states of the collinear AFM-s state from the collinear spin-polarized GGA+U calculations.

atoms.

Finally, we ploted the electronic band structure and densities of states of the most stable non-collinear AFM state (θ=107° in Table 5.4) we found in Figure 5.18 and 5.19. The lowest valence band at the Γ point is Cu1-$d_{x^2-y^2}$ and Cu1-d_{xy} dominant bands hybridized with O1-p_y orbitals at −6.6 eV with a narrow bandwidth of about 0.2 eV. Bands dominated by Cu2-d_{z^2} orbital hybridized with O1-p_z and O6-p_z orbitals near −6.4 eV in the collinear AFM state slightly rise to about −6.3 eV here. And, bands dominated by Cu3-$d_{x^2-y^2}$ orbital hybridized with O5-p_x orbital and Cu3-d_{zx} orbital hybridized with O1-p_x orbital slightly drop to about −6.1 eV. Above −6 eV and below −0.5 eV, bands are too complex to be recognized. Likewise, the highest occupied band with narrow bandwidth of about 0.1 eV is dominated by Cu1-d_{zx} orbital hybridized with O2-p_z and O3-p_x orbitals, and Cu1-d_{z^2} orbital hybridized with O2-p_z orbital. The energy gap increase further to 1.47 eV. In the intervals between 1.4 eV and 1.8 eV, there is a series of narrow conduction bands. The lowest bands in the vicinity of 1.43 eV are dominated by Cu3-$d_{x^2-y^2}$ and Cu3-d_{zx} orbitals. The bands dominated by Cu2-d_{z^2} orbital slightly hybridized with O1-p_z orbital near 1.63 eV in the collinear AFM state drop to 1.61 eV here. The highest band in the vicinity of 1.75 eV is dominated by Cu1-$d_{x^2-y^2}$ and Cu1-d_{xy} orbitals. Above 3 eV, bands are dominated by orbitals of Mo atoms hybridized with p-orbitals of the surrounding O atoms. As the angle is rotated away from $\theta = 107°$ and 287°, the energy gap decrease gradually to 1.44 eV which correspond to $\theta = 197°$ and 17° approximately. With and without considering

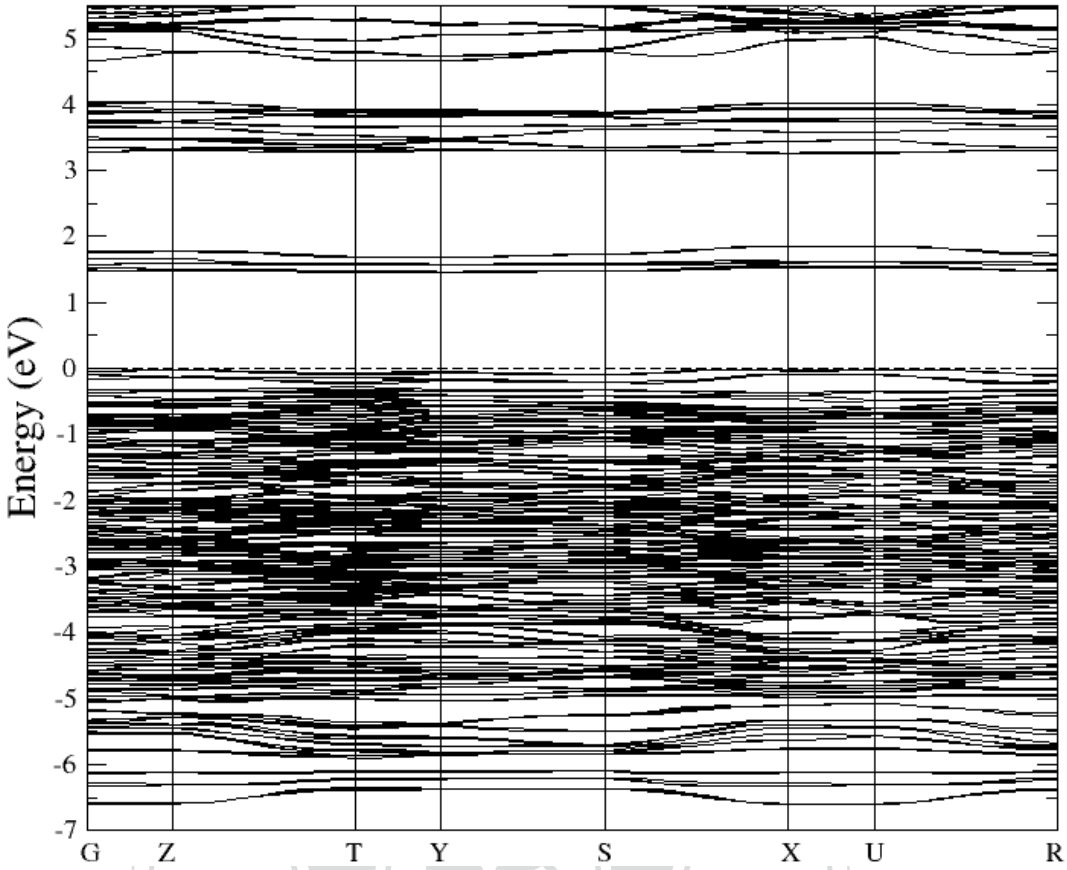

Figure 5.18: The electronic band structure of the most stable non-collinear AFM state ($\theta = 107^\circ$ or 287° approximately) we found from GGA+U calculation with spin-orbit coupling.

the relativistic effect do not make considerable difference in the electronic band structure and densities of states.

5.6 Spontaneous Electric Polarization

The $Cu_3Mo_2O_9$ has been found by Kuroe et al. [37] to have remarkable magnetoelectric effect, being as strong as that of $TbMnO_3$. A small spin cluster model has been suggested which is different from the magnetic superlattice. Since there has been no *ab initio* calculation yet, we performed the Berry's phase calculations to obtain the theoretical spontaneous electric polarization for $Cu_3Mo_2O_9$. As is mentioned before, the electric polarization can appear when the spatial inversion symmetry of the system is broken. Such breaking can be caused by crystal structure distortion or the special spin configuration. In the $Cu_3Mo_2O_9$, the electric polarization is caused by the breaking of the inversion symmetry of spin configuration. We calculated the polarization of the most stable noncollinear AFM state we found ($\theta = 107^\circ$ approximately) with considering the relativistic effect. A theoretical value ($\simeq$866.58 $\mu C/m^2$) is in the same order of experimental results. However, the direction is different from the experimental one. The experimental results reveal that the spontaneous polarization appears ($\simeq$500 $\mu C/m^2$) along c-axis,

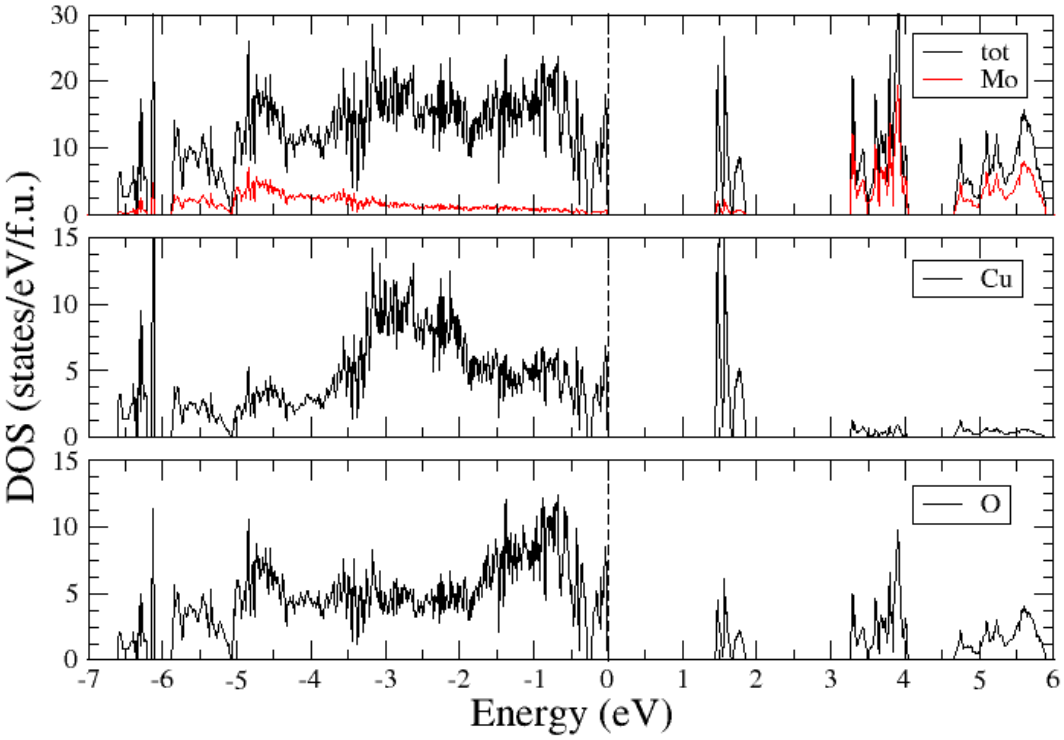

Figure 5.19: Total and site-projected electronic densities of states of the most stable non-collinear AFM state we found from GGA+U calculation with spin-orbit coupling.

but our theoretical polarization is along *b*-axis. We look into the most stable spin configuration we found to try to realize the system further. Spins on Cu-sites are listed in Table 5.5. The Cu1 ions are located on the symmetric center of the system, direction of spin on Cu1 does not affect the spatial symmetry of the system. Cu2-1 and Cu2-2 are spatial symmetric sites of Cu2-4 and Cu2-3 respectively, and Cu3-1 and Cu3-2 are spatial symmetric cites of the Cu3-4 and Cu3-3 respectively. We inspected directions of spins in the most stable state we found. Spins on Cu2-1 and Cu2-4 point to oppsite directions in the x and z components. And, spins on Cu2-2 and Cu2-3 (Cu3-1 and Cu3-4, Cu3-2 and Cu3-3) also point to oppsite directions in the x and z components. The spatial inversion symmetry is broken in the direction lie in the xz-plane. However, the spontaneous electricpolarization appears along the b-axis, which does not agree with our expectation. In our opinion, there are some possible explanations for dealing with the disagreement of direction of the electric polarization between experimental results and our calculations. First, the direction of polarization found by Kuroe et al. is wrong. Second, the electron-electron Coulomb repulsion has been considered on every Cu sites with the commonly used values of $U = 4.5$ eV and $J = 0.9$ eV in our calculations. However, there are three crystallographically inequivalent Cu ions. The Hubbard U on crystallographically different Cu sites may have different values. Third, since the DFT+U method is still a single particle method, it may be probably insufficient to deal with the strong correlated many-body behavior. Forth, since the magnetic structure is still not well determined, the spin configuration we found is probably not the magntic structure of the ground state.

Table 5.8: A spin configuration that the theoretical electric polarization of the state agrees with the experimental results. Spin-orbit coupling has been considered. Energy (meV/unit cell), band gap (eV) and spin moments (μ_B) on Cu ions are listed.

energy	11.98		
gap	1.36		
Cu1-1	0.105	0.606	0.114
Cu1-2	-0.174	-0.585	0.131
Cu1-3	-0.170	-0.585	-0.137
Cu1-4	0.109	0.606	-0.109
Cu2-1	-0.013	0.650	0.059
Cu2-2	-0.084	0.644	0.057
Cu2-3	0.086	-0.645	-0.022
Cu2-4	0.010	-0.644	-0.096
Cu3-1	0.166	0.626	0.155
Cu3-2	0.176	0.623	-0.154
Cu3-3	-0.155	-0.635	0.131
Cu3-4	-0.146	-0.637	-0.132

In addition to the results above, we have found a spin configuration that the theoretical electric polarization of the state agrees with the experimental results. However, the symmetry of the spin configuration does not satisfy the conditions suggested by results of the neutron diffraction experiment. And, spins on neighboring Cu2 and Cu3 do not form a singlet dimer. The spin configuration is listed in Table 5.8. We can see that all spins mainly point along b-axis. The polarization (only $\simeq$31 μC/m^2) appears along c-axis. We hope that our calculated results can contribute to the studies of $Cu_3Mo_2O_9$.

Chapter 6

Summary and Conclusions

We have done a series of *ab initio* calculations to study the interesting material, $Cu_3Mo_2O_9$, which reveals strong magnetoelectric effect. There has no *ab initio* study of it and its magnetic structure is still not well defined. Our *ab initio* calculations are based on spin density functional theory with generalized gradient approximation (GGA). We used the accurate full-potential projector augmented-wave (PAW) method, as implemented in the VASP code. The core radii of the copper, molybdenum and oxygen atoms are 1.312, 1.455 and 0.8, respectively.

In our GGA calculations, the NM and the FM states are matallic. Though a gap ($\sim$0.2 eV) opens in collinear AFM state, it is too small to agree with the crystal field theory. Since $Cu_3Mo_2O_9$ was prepared as a brown-orange powder, the absorbed energy corresponding to the complementary color of visible light must be at least 1.0 eV, i.e. the energy gap must be at least 1.0 eV. Though results of neutron diffraction experiments reveal that the magnetic structure of $Cu_3Mo_2O_9$ probably be non-collinear, rather than our collinear configurations, the effects of exchange interaction are insufficient to open a wide enough gap. Furthermore, the spin moments on Cu ions are much smaller than the theoretical value (1.0 μ_B). Therefore, we can have a conclusion that the electron-electron Coulomb repulsion in the system must be considered. The GGA+U method consists in Hubbard-like correction gives a good description of electronic correlation with the commonly used values of $U = 4.5$ eV and $J = 0.9$ eV so that a reasonable band gap could be obtained.

In our GGA+U calculations, a reasonable gap was obtained. The most stable state we found is the AFM-s state with a largest gap of 1.472 eV in our calculations. The noncollinear AFM spin configurations we found are similar to results of neutron diffraction experiments. When we do not consider the relativistic effect, all spins lie in the *ac*-plane. Spins on Cu1 form an AFM chain. Spins on Cu2 and Cu3 form a singlet dimer weakly interacting with the AFM chain formed by Cu1 ions. The most stable noncollinear AFM state we found is that an angle $\theta = 107^\circ$ and 287° approximately appear between *a*-axis and direction of spin of Cu1. The energy gap is 1.47 eV. As spins on Cu1 are rotated away from $\theta = 107^\circ$ and 287°, the energy gap decrease gradually to 1.44 eV when $\theta = 197^\circ$ and 17°. As we consider the relativistic effect, all

spins still lie in the *ac*-plane almost in the most stable spins configuration. However, when spins on Cu1 rotating to another angle, the spins cant away from the *ac*-plane, especially on Cu1. The *b*-component of spin moments on Cu1 increase gradually to the upper limit (about 7% of spin moment) when $\theta = 197^\circ$ and 17°.

To obtain the theoretical exchange parameters (J_1, J_2, J_3, J_4 and J_5) of the system, a series of collinear spin-polarized calculations with different spin configurations have been performed. Two of exchange parameters (J_1 and J_5) in our results are positive, and the remaining (J_2, J_3 and J_4) are negative. Our results agree with the experimental results well. We think that the exchange interactions tend to make spins lie in the *ac*-plane, and the relativistic effect tends to make spins point along the *b*-axis. Since the relativistic effect is fixed, when spins on Cu1 are rotated away from the most stable pointings, the dominance of exchange interactions decrease and *b*-component of spins increase.

We analysed the electronic band structure and densities of states of NM, collinear FM, AFM-s and AFM-t, and the most stable noncollinear AFM states (GGA+U). The NM state is metallic. When considering the spin-polarization, some transfering of electrons occur, and a series of conduction band appear in the vicinity of 1.5 eV. These conduction bands are effects of considering Coulomb repulsion of electrons. An electron can occupy one these bands only if it overcomes the Hubbard U from another electron in the band. We can see that the bandwidth in AFM states (both collinear and noncollinear) are narrow than the collinear FM state. And, the apparent shifts occur between collinear and noncollinear states in the vicinity of 1.5 eV.

We also have done the Berry's phase calculations with considering the relativistic effect. The strength of theoretical spontaneous electric polarization of the most stable state we found ($\simeq$866.58 μC/m^2) agrees with the results of experiments ($\simeq$500 μC/m^2). However, the directions are different. The polarization measured by Kuroe et al. is along the *c*-axis, but along the *b*-axis in our calculations. In our opinion, there are some possible explanations for dealing with the different directions of the electric polarization between experimental and our results. First, the direction of polarization measured by Kuroe et al. is wrong. Second, the electron-electron Coulomb repulsion has been considered on every Cu sites with the commonly used values of $U = 4.5$ eV and $J = 0.9$ eV in our calculations. However, there are three crystallographically inequivalent Cu ions. The Hubbard U on crystallographically different Cu sites may have different values. Third, since the DFT+U method is still a single particle method, it may be probably insufficient to deal with the strong correlated many-body behavior. Forth, since the magnetic structure is still not well determined, the spin configuration we found is probably not the magntic structure of the ground state.

In addition to the results above, we have found a spin configuration that the theoretical electric polarization ($\simeq$31 μC/m^2 along c-axis) of the state agrees with the experimental results. However, the symmetry of the spin configuration does not satisfy the conditions suggested by results of the neutron diffraction experiment. And, spins on neighboring Cu2 and Cu3 do not form a singlet dimer.

The theoretical electric polarization in our calculations does not completely agree with experimental results. Nevertheless, the spin configurations, theoretical exchange parameters have been obtained in our calculations. And, the electronic structure has been analysed. We hope that our results can help those who wants to study this interesting material further.

References

[1] P. Hohenberg and W. Kohn, "*Inhomogeneous Electron Gas*", Phys. Rev. **136**, B864 (1964).

[2] W. Kohn and L. J. Sham, "*Self-Consistent Equations Including Exchange and Correlation Effects*", Phys. Rev. **140**, A1133 (1965).

[3] M. Born and J. R. Oppenheimer, "*On The Quantum Theory of Molecules*", Ann. Physik **84**, 457 (1927).

[4] L. H. Thomas, "*The Calculation of Atomic Fields*", Proc. Camb. Phil. Soc. **23**, 542 (1927).

[5] J. P. Perdew and A. Zunger, "*Self-interaction correction to density-functional approximations for many-electron systems*", Phys. Rev. B **23**, 5048 (1981).

[6] J. P. Perdew, J. A. Chevary, S. H. Vosko, K. A. Jackson, M. R. Pederson, D. J. Singh, and C. Fiolhais, "*Atoms, Molecules, Solids, and Surfaces: Applications of The Generalized Gradient Approximation for Exchange and Correlation*", Phys. Rev. B 46, 6671 (1992); 48, 4978(E)(1993).

[7] J. P. Perdew, K. Burke, and M. Ernzerhof, "*Generalized Gradient Approximation Made Simple*", Phys. Rev. Lett. **77**, 3865 (1996).

[8] J. H. de Boer and E. J. W. Verwey, "*Semi-Conductors with Partially and with Completely Filled 3d-Lattice Bands*", Proc. Phys. Soc. **49**, 59 (1937).

[9] J. Hubbard, "*Electron Correlations in Narrow Energy Bands.*", Proc. Roy. Soc. A **276**, 238 (1963).

[10] J. Hubbard, "*Electron Correlations in Narrow Energy Bands. III. An Improved Solution*", Proc. Roy. Soc. A **281**, 41 (1964).

[11] A. Svane and O. Gunnarsson, "*Transition-Metal Oxides in The Self-Interaction-Corrected Density-Functional Formalism*", Phys. Rev. Lett. **65**, 1148 (1990).

[12] S. Massidda, M. Posternak and A. Baldereschi, "*Hartree-Fock LAPW Approach to The Electronic Properties of Periodic Systems*", Phys. Rev. B **48**, 5058 (1993).

[13] L. Hedin, "*New Method for Calculating The One-Particle Green's Function with Application to the Electron-Gas Problem*", Phys. Rev. **139**, A796 (1965).

[14] A. I. Liechtenstein, V. I. Anisimov and J. Zaanen, "*Density-Functional Theory and Strong Interactions: Orbital Ordering in Mott-Hubbard Insulators*", Phys. Rev. B **52**, R5467 (1995).

[15] S. L. Dudarev, G. A. Botton, S. Y. Savrasov, C. J. Humphreys and A. P. Sutton, "*Electron-Energy-Loss Spectra and The Structural Stability of Nickel Oxide:An LSDA+U Study*", Phys. Rev. B **57**, 1505 (1998).

[16] H. Bethe, "*Splitting of Terms in Crystals*", Ann. Physik **3**, 133 (1929).

[17] J. H. Van Vleck, "*Theory of The Variations in Paramagnetic Anisotropy Among Different Salts of The Iron Group*", Phys. Rev. **41**, 208 (1932).

[18] H. A. Jahn and E. Teller, "*Stability of polyatomic Molecules in Degenerate Electronic States. I. Orbital Degeneracy*", Proc. Roy. Soc. A **161**, 220 (1937).

[19] J. Springborg and C. E. Schaffer, "*Tetrakis (pyridine) Cobalt(III) Complexes*", Acta. Chem. Scand. **27**, 3312 (1973).

[20] L. D. Landau and E. M. Lifshitz, *Electrodynamics of continuous media* (Fizmatgiz, Moscow, 1959).

[21] E. Ascher, H. Rieder, H. Schmid and H. Stossel, "*Some Properteis of Ferromagnetoelectric Nickel-Iodine Boracite, $Ni_3B_7O_{13}I$*", J. Appl. Phys. **37**, 1404 (1966).

[22] J. Wang, J. B. Neaton, H. Zheng, V. Nagarajan, S. B. Ogale, B. Liu, D. Viehland, V. Vaithyanathan, D. G. Schlom, U. V. Waghmare, N. A. Spaldin, K. M. Rabe, M. Wuttig and R. Ramesh, "*Epitaxial $BiFeO_3$ Multiferroic Thin Film Heterostructures*", Science **299**, 1719 (2003).

[23] N. Hur, S. Park, P. A. Sharma, J. S. Ahn, S. Guha and S-W. Cheong, "Electric Polarization Reversal and Memory in A Multiferroic Material Induced by Magnetic Fields", Nature **429**, 392 (2004).

[24] T. Kimura, T. Goto, H. Shintani, K. Ishizaka, T. Arima and Y. Tokura, "*Magnetic Control of Ferroelectric Polarization*", Nature **426**, 55 (2003).

[25] G. Toulouse, "*Theory of The Frustration Effect in Spin Glasses I*", Commun. Phys. **2**, 115 (1977).

[26] J. Vannimenus and G. Toulouse, "*Theory of The Frustration Effect. II. Ising Spins on A Square Lattice*", J. Phys. C: Solid State Phys. **10**, L537 (1977).

[27] G. H. Wannier, "*Antiferromagnetism. The Triangular Ising Net*", Phys. Rev. **79**, 357 (1950).

[28] L. Pauling, "*The Structure and Entropy of Ice and of Other Crystals with Some Randomness of Atomic Arrangement*", J. Am. Chem. Soc. **57** 2680 (1935).

[29] N. A. Hill, "*Why Are There so Few Magnetic Ferroelectrics?*", J. Phys. Chem. B **104**, 6694 (2000).

[30] D. I. Khomskii, "*Multiferroics: Different Ways to Combine Magnetism and Ferroelectricity*", J. Magn. Magn. Mater. **306**, 1 (2006).

[31] D. V. Efremov, J. van den Brink, and D. I. Khomskii, "*Bond-Versus Site-Centred Ordering and Possible Ferroelectricity in Manganites*", Nature Mater. **3**, 853 (2004).

[32] B. B. Van Aken, T. T. M. Palstra, A. Filippetti and N. A. Spaldin, "*The Origin of Ferroelectricity in Magnetoelectric $YMnO_3$*", Nature Mater. **3**, 164 (2004).

[33] D. Khomskii, "*Classifying Multiferroics: Mechanisms and Effects*", Physics **2**, 20 (2009).

[34] H. Katsura, N. Nagaosa and A. V. Balatsky, "*Spin Current and Magnetoelectric Effect in Noncollinear Magnets*", Phys. Rev. Lett. **95**, 057205 (2005).

[35] M. V. Mostovoy, "*Ferroelectricity in Spiral Magnets*", Phys. Rev. Lett. **96**, 067601 (2006).

[36] M. Fiebig, "*Revival of The Magnetoelectric Effect*", J. Phys. D **38**, R123 (2005).

[37] H. Kuroe, T. Hosaka, S. Hachiuma, T. Sekine, M. Hase, K. Oka, T. Ito, H. Eisaki, M. Fujisawa, S. Okubo and H. Ohta, "*Electric Polarization Induced by Neel Order without Magnetic Superlattice: Experimental Study of $Cu_3Mo_2O_9$ and Numerical Study of A Small Spin Cluster*", J. Phys. Soc. Jpn. **80**, 083705 (2011).

[38] S. Vilminot, G. Andre and M. Kurmoo, "*Magnetic Properties and Magnetic Structure of $Cu_3Mo_2O_9$*", Inorg. Chem, **48**, 2687 (2009).

[39] T. Hamasaki, T. Ide, H. Kuroe and T. Sekine, "*Successive Phase Transitions to Antiferromagnetic and Weak-Ferromagnetic Long-Range Order in The Quasi-One-Dimensional Antiferromagnet $Cu_3Mo_2O_9$*", Phys. Rev. B **77**, 134419 (2008).